

ABSTRACT

Title of Thesis: CHARACTERIZATION OF METAL-OXIDE SEMICONDUCTOR SENSORS FOR R-32 AND R-454B LEAKS

Garrett Wack, Master of Science, 2020

Thesis Directed By: Professor Peter B. Sunderland, Department of Fire Protection Engineering

Owing to concerns about climate change, California and several other states have passed laws phasing out high global warming potential refrigerants in HVAC and refrigeration systems. In the near term, the most likely replacements are A2L (mildly flammable) refrigerants. Area monitoring detectors will be required for most future residential, commercial, and industrial HVAC systems that use A2L refrigerants. These detectors must operate continuously, preferably without service for many years. The UL 60335-2-40 (2019) standard requires these detectors to respond within 10 s to a concentration of 100% of the LFL. Inexpensive detectors that meet these requirements have been slow to develop which has delayed the adoption of A2L refrigerants. A technology with good potential is based on metal-oxide semiconductors (MOS). MOS detectors from Figaro are tested here, considering their response to leaks of R-32 and R-454B. They are characterized according to sensitivity, response time, recovery time, and poisoning. The sensors do not satisfy the 10 s response time for R-32 or R-454B at

the 25% LFL equivalent voltage, but succeed at the 10% LFL equivalent voltage. Their steady-state output is linear with respect to the logarithm of concentration. However, both response time and linearity are subject to possible poisoning and aging. Although the MOS sensor performance is generally acceptable, poisoning and lifetime remain a concern.

CHARACTERIZATION OF METAL-OXIDE SEMICONDUCTOR SENSORS
FOR R-32 AND R-454B LEAKS

by

Garrett Wack

Thesis submitted to the Faculty of the Graduate School of the
University of Maryland, College Park, in partial fulfillment
of the requirements for the degree of
Master of Science
2020

Advisory Committee:

Professor Peter B. Sunderland, Chair

Professor James A. Milke

Associate Professor Stanislav I. Stoliarov

© Copyright by
Garrett Wack
2020

Acknowledgements

There are a number of people I would like to thank for helping me with this research project. First and foremost, I would like to thank Dr. Peter Sunderland for giving me this opportunity and advising me throughout the course of this research. I could not imagine working with a more knowledgeable, level-headed advisor, and I am truly honored. I am grateful for you always taking the time to ask about my life outside of research and school, and hope that I can take with me your positive attitude and work ethic wherever I go.

Secondly, I would like to thank Carrier for their financial support on this project and providing me this opportunity to pursue my higher education. I would specifically like to extend my gratitude to Michael Birnkrant and Marcin Piech for their leadership on the project. You were always respectful of the fact that I was balancing my research with classwork, and were easily approachable when I had questions. Special thanks to you and Sarath Srikakulapu for helping me in the lab as well.

Next, I would like to thank all of the FPE faculty and students whom made my graduate school experience amazing. To all of the students, for sharing the lab space and providing me with a helpful hand when I needed one. I will never forget all of the great conversations we had that helped to take my mind off of the stresses of life. To Dr. Gollner, for sharing his lab space with ours and allowing me to borrow chemicals for testing. To Fernando, for running and maintaining all of the lab spaces and for helping me to find necessary equipment and chemicals. Special thanks to Dr. Milke and Dr. Stas for serving on my thesis committee.

Lastly, I would like to thank all my friends and family for their unwavering love and support throughout this past year. To my friends, for all the fun conversations, interactions, and trips that gave me a chance to enjoy and appreciate the little things. To my siblings, for providing me with entertainment around the house and helping to take my mind off work. Most importantly, to my parents, for everything you have done for me and ensuring one of the busiest years of my life was a fun one as well. I cannot express how much I appreciate the comfortable environment of our house, the home-cooked meals waiting for me every night when I got back from school, and for always going out of your way to make sure I am doing alright.

Table of Contents

List of Tables	v
List of Figures	vi
Chapter 1: Introduction	1
1.1 Motivation	1
1.2 Objectives	3
1.3 Literature Review	4
1.3.1 Comparison of Available Sensing Technologies	4
1.3.1.1 Selection of Sensing Technology	12
1.3.2 Introduction to MOS Technology	12
1.3.3 Comparison of Available MOS Sensors	15
1.3.3.1 Selection of Sensor	17
Chapter 2: Experimental	19
2.1 Sensor Specifications	19
2.2 Sensor Setup	21
2.3 Test Apparatus	24
2.4 Effect of Humidity	27
2.5 Soap Bubble Calibration	29
Chapter 3: Response to Refrigerant Leaks	33
3.1 Plunge Tests	33
3.2 Response Time Tests	39
Chapter 4: Contaminant Tests	43
4.1 Contaminant Test Procedure	43
4.2 State of Health Tests	46
4.3 Gas Contaminants	47
4.4 Liquid Contaminants	48
4.5 Results	53
4.6 Discussion of Results	63
Chapter 5: Conclusions and Future Work	67
Bibliography	70

List of Tables

1.1 Refrigerant classification scheme. Reproduced from [1]	2
1.2 Commercially available refrigerant sensing technologies	6
1.3 Failure mode ranking, reproduced from [2].....	8
1.4 Failure mode ranking for commercial/industrial applications, reproduced from [2]	9
1.5 Failure mode ranking for residential applications, reproduced from [2]	9
1.6 Suitability to certain refrigerants, reproduced from [3]	11
2.1 FCM2630-C00 pin connections, reproduced from [4]	20
3.1 Voltage differences at various concentrations of refrigerant, V	36
3.2 Sensor response time to 25% LFL, s	40
3.3 Sensor response time to 10% LFL, s	40
4.1 Contaminants and concentrations required for testing, reproduced from [5]	44
4.2 Acquired contaminants	44
4.3 Gas concentrations and flow rates for determining air-to-contaminant ratio	48
4.4 Properties of water	51
4.5 Properties of contaminants.....	52
4.6 Mass loss rates and flowrates for liquid contaminants	53
4.7 Summary of the contaminant's effect on the sensor	66

List of Figures

1.1 Schematic band diagrams of an insulator, semiconductor, and conductor. Reproduced from [6].....	14
1.2 Schematic diagram of band bending. Reproduced from [7].....	15
1.3 Commercially available MOS sensors, reproduced from [4], [8-10]	17
2.1 FCM2630-C00 structure and dimensions, reproduced from [4].....	19
2.2 Actual FCM2630-C00 sensor module with connected wires	21
2.3 Wiring arrangement	22
2.4 Wiring schematic	23
2.5 LabVIEW user interface	24
2.6 Test apparatus	25
2.7 Test apparatus schematic	26
2.8 Nalgene 500 mL vessel.....	27
2.9 Effect of humidity.....	28
2.10 Filtering flask assembly	28
2.11 Soap bubble flowmeters.....	30
2.12 Calibrated flowrates as a function of ball height	31
3.1 Sensor response to increasing refrigerant concentration steps at (a) 0% LFL, (b) 10% LFL, (c) 25% LFL, (d) 75% LFL, and (e) 100% LFL	35
3.2 Voltage difference for various concentrations of R-32.....	38
3.3 Voltage difference for various concentrations of R-32 on a logarithmic scale	38
3.4 Response time test for R-32.....	41
3.5 Response time test for R-454B	41
4.1 Bubbling apparatus	50
4.2-14 Results of the contaminant and state of health test.....	54-62
4.15 Chronological summary of contamination and state of health test results	63
4.16 Summary of response times from fastest to slowest.....	65
4.17 Response time following contaminant testing	65
5.1 Time constant from the response time test for R-32.....	68

Chapter 1: Introduction

1.1 Motivation

Owing to concerns about climate change, California and several other states have passed laws phasing out high global warming potential (GWP) refrigerants in HVAC and refrigeration systems. Hydrofluorocarbons (HFCs) are currently the most common type of refrigerant found in such systems. While they have low toxicity and are non-flammable, they have high GWP values ranging from 1,430 to 3,985 [11]. In recognizing the harmful effects these refrigerants have on the environment, the industry has started transitioning to less damaging, lower-GWP HFC alternatives [2].

These proposed climate-friendly alternatives have been in recent development over the last few years, and are known as A2L refrigerants. A2L refrigerants are mildly flammable, but have much lower GWP values that range from 4 to 675 [1]. The A2L classification is an ASHRAE created safety category for refrigerants that meet the specifications of A2 (lower flammability), but also have a burning velocity of ≤ 10 cm/s while tested at 23 °C and 101.3 kPa [12]. Several of these refrigerants are either pure HFC-32 or blends of HFC-32, HFO-1234yf or HFO-1234ze [13]. Table 1.1 summarizes the refrigerant classification scheme and shows how A2L compares to other classifications. The vast majority of HFC refrigerants commonly used now are classified as A1 [1].

Table 1.1. Refrigerant classification scheme. Reproduced from [1].

A3	B3	Higher Flammability
A2	B2	Flammable
A2L	B2L	Lower Flammability
A1	B1	Non-Flammable
Lower Toxicity	Higher Toxicity	

As early as 2023, California plans on banning the use of greenhouse refrigerant gases with a GWP value of ≥ 750 in new residential and commercial HVAC and refrigeration systems [14]. Although A2L refrigerants meet this proposed regulation, their flammability still presents a fire hazard that is not too well understood. Therefore, area monitoring sensors will be required for most future residential, commercial, and industrial HVAC systems that use A2L refrigerants.

Sensors for A2L refrigerant leaks are available, but are generally too expensive for residential applications. For example, sensors used in machinery rooms typically cost \$3,000 – \$5,000 each. The target cost in residential applications is far lower, preferably below \$10. Regular sensor calibrations are not practical; at least 5 years (preferably 15) without maintenance is necessary. Annex LL, Section 3 of the UL 60335-2-40 (2019) standard requires these sensors to respond within 10 s to a concentration of 100% of the refrigerant’s lower flammability limit (LFL), which may be hard to obtain. Finally, the standard also requires the sensor to continue to perform healthily after being exposed to a prescribed list of contaminants that could potentially be found in air, as well as not return a false alarm [5]. Inexpensive detectors that meet

these requirements have been slow to develop which has delayed the adoption of A2L refrigerants.

1.2 Objectives

The focus of this research is to identify a suitable sensing technology for A2L refrigerant gas detection in residential HVAC systems. The first challenge is finding a relatively inexpensive sensor that can be tested using a lab with limited space. An apparatus then needs to be built to proceed with testing. Two main sensor performances were prioritized for testing. The first is determining the sensor's response time to 100% of the LFL of A2L refrigerant, and if it is lower than 10 s. R-32 and R-454B were the chosen A2L refrigerants to test with. The second is how the sensor responds to exposure to various contaminants that can be found in a typical residential setting and become air-born.

A literature review was conducted to review and compare available sensing technologies to identify one or more inexpensive, durable sensors that could potentially succeed with the two tests identified. A technology found to have good potential is based on metal-oxide semiconductor (MOS) sensors. MOS sensors from Figaro were then acquired and tested. To test, an apparatus was constructed that could deliver a mixture of refrigerant and the various contaminants with air at different concentrations. Repeated calibration and testing was done to perfect a technique that delivered the sensors quickly to as close to the desired concentration as possible. The sensors were then characterized according to sensitivity, response time, recovery time, and poisoning.

The objectives of this study are to:

- Identify a suitable commercially available sensing technology
- Identify a suitable commercially available sensor
- Acquire the sensor
- Construct an experimental apparatus to test the sensor
- Test the sensor with refrigerant to characterize the response time
- Test the sensor with contaminants to characterize recovery time and poisoning

1.3 Literature Review

The purpose of this literature review is to gain insight into existing gas sensing technologies in order to meet the research goals of this thesis. First, a number of refrigerant detection methods are reviewed and compared. The extensive list is then narrowed down to identify a sensing technology that could realistically perform under the desired expectations. The chosen technology is researched to gain insight into the principles behind the science. Finally, available sensors of the chosen technology are compared and contrasted in order to select one (or multiple) to acquire and test.

1.3.1 Comparison of Available Sensing Technologies

Following a new regulation to reduce CFC production by 50%, McClure and Anderson (1990) [15] reviewed potential leak monitoring methods to minimize losses and costs. The three methods reviewed were gas ionization, infrared absorption, and metal-oxide semiconductor (MOS). They concluded that MOS sensors were most appropriate for smaller spaces, while infrared absorption would work well for larger

spaces, such as commercial and industrial areas. Tapscott and Sohn (1996) [16] present an extensive list of halocarbon refrigerant detection methods for the US Army Corps of Engineers. In recognition of the eventual phase out of a significant number of high GWP refrigerants that the U.S. Army used, their goal was to compile and assess a number of technologies that could possibly be used to detect newer low GWP refrigerants.

Table 1.2 summarizes these technologies according to the sensor selectivity. Refrigerant sensors can be categorized into three classes of selectivity, which are nonselective, halogen-selective, and compound-selective. Nonselective sensors can detect a wide range of gases, even those that are not refrigerants. Halogen-selective sensors can only detect compounds with halogen atoms, and compound-specific sensors are pre-set to detect a few specified refrigerants [16].

As the selectivity of the sensor increases, so does the cost and complexity. Therefore, the nonselective group is the most appealing as long as the sensor can succeed with the contaminant testing. Tapscott and Sohn [16] state that flame ionization is not a common method for area monitoring refrigerant leaks, and its application has yet to be proven. Gas-membrane galvanic cell sensors work well with HCl detection, but experience interference from other acid gases for HF detection. Negative corona discharge sensors detect gases containing halogen the best, but detect other gases as well. They have a quick response, and are employed widely in HVAC equipment to pinpoint leaks.

Table 1.2. Commercially available refrigerant sensing technologies.

Technology	Principle
<i>Nonselective</i>	
Flame ionization	Gas is pulled into a hydrogen flame. Ionized gas is detected with an electrode. Gases with carbon will emit signal.
Gas-membrane galvanic cell	Gas is pyrolyzed by a hot filament. Product passes through a membrane and is absorbed onto an electrode. Redox reaction on counter electrode results in a current equivalent to gas concentration.
Negative corona discharge	Two electrodes are exposed to atmosphere in a housing. Housing becomes ionized. Gas changes the dielectric breakdown potential. Resulting current change creates signal.
Solid state	Gas changes the resistivity of heated metal-oxide semiconductor.
Thermal conductivity	Gases conduct heat differently than air. Contaminants are identified from thermal conductivity of mixture.
<i>Halogen-Specific</i>	
Electron capture	Radioactive source creates electron flow. Gas enters sensor and removes electrons from flow. Decrease in current activates signal.
Heated diode	Gas is thermally decomposed. Halogen atoms react with alkali metal atoms. Resulting ion current measures concentration of gas.
<i>Compound-Specific</i>	
Gas chromatography	Gas mixture is separated. Individual components are identified.
Infrared (IR)	Beam of infrared radiation is passed through gas. Absorption is determined at selected wavelengths.
Mass spectra-based	Gas is scanned for specified mass peaks to identify a certain gas.

The most common solid state sensors use MOS technology. MOS sensors are inexpensive compared to other technologies, require infrequent calibration, and have the possibility of lasting more than 5 years. However, response time can be slower to lower refrigerant concentrations, and they are possibly subject to interference by other gases.

Thermal conductivity sensors have a low sensitivity to various compounds, so the response time could be slow, but a few companies still manufacture this type of sensor [16].

According to Tapscott and Sohn [16], negative corona discharge sensors are the most commonly used sensors for pinpointing leaks. However, sensors used for area monitoring is what is being sought in this thesis. The most common sensor type used for area monitoring are solid state and IR sensors. IR sensors have a higher sensitivity, but are much more expensive. Solid state sensors are a much more affordable option, but have a lower selectivity and sensitivity. Although Tapscott and Sohn [16] present a complete review of commercially available refrigerant detection methods, these technologies have been much more developed in the past 20 years.

Wagner and Ferenchaick (2017) [2] focus on current sensing technologies that could meet the proposed requirements for detecting A2L refrigerants. They narrow the list of technologies presented in Table 1.2 down to four: IR, electrochemical (EC), solid state, and heated diode. EC sensors work very similarly to gas-membrane galvanic cell sensors. Solid state sensors are divided into two different technologies: MOS and catalytic-type. Similar to MOS sensors, catalytic-type sensors respond to changes in resistance on a catalytic surface. Flammable gases are oxidized on the catalytic surface

which releases heat. The heat increases the resistance on the circuit that the sensing element is on. The resultant voltage increase directly correlates to a concentration of flammable gas [2].

Wagner and Ferenchaick [2] considered a number of different ways that the sensors could fail in various settings. A failure mode ranking system shown in Table 1.3 [2] assigned a score to each technology based on the likelihood and severity for each failure mode considered. High scores indicate the failure mode will have a large impact on the safety and operation of the sensor. Tables 1.4 and 1.5 [2] summarize the scores for each technology for commercial/industrial and residential applications, respectively. Other failure modes do exist, but they were not included due to difficulty in quantifying them.

Table 1.3. Failure mode ranking, reproduced from [2].

		Severity				
		Not Applicable (NA)	Low (L)	Moderately Low (ML)	Moderately High (MH)	High (H)
Likelihood	Not Applicable (NA)	0	-	-	-	-
	Unlikely (U)	-	2	3	4	5
	Moderately Unlikely (MU)	-	3	4	5	6
	Moderately Likely (ML)	-	4	5	6	7
	Likely (L)	-	5	6	7	8

Table 1.4. Failure mode ranking for commercial/industrial applications, reproduced from [2].

Failure Mode		IR		EC		MOS		Catalytic		Heated Diode	
Humidity	Likelihood	U	3	MU	5	U	4	U	2	L	7
	Severity	ML		MH		MH		L		MH	
Temperature	Likelihood	U	3	U	3	MU	4	MU	3	U	2
	Severity	ML		ML		ML		L		L	
False Triggering Gases	Likelihood	NA	0	ML	6	ML	5	NA	0	ML	5
	Severity	NA		MH		ML		NA		ML	
Poisoning or Blocking Gases	Likelihood	ML	4	ML	6	U	2	ML	5	NA	0
	Severity	L		MH		L		ML		NA	
Overexposure	Likelihood	U	2	L	6	ML	5	ML	5	ML	5
	Severity	L		ML		ML		ML		ML	
Air Contaminants	Likelihood	U	3	U	2	MU	3	MU	3	U	2
	Severity	ML		L		L		L		L	
Total		15		28		23		18		21	

Table 1.5. Failure mode ranking for residential applications, reproduced from [2].

Failure Mode		IR		EC		MOS		Catalytic		Heated Diode	
Humidity	Likelihood	U	3	U	4	U	4	U	2	U	4
	Severity	ML		MH		MH		L		MH	
Temperature	Likelihood	U	3	U	3	U	3	U	2	U	2
	Severity	ML		ML		ML		L		L	
False Triggering Gases	Likelihood	NA	0	MU	5	U	3	NA	0	MU	4
	Severity	NA		MH		ML		NA		ML	
Poisoning or Blocking Gases	Likelihood	MU	3	ML	6	U	2	ML	5	NA	0
	Severity	L		MH		L		ML		NA	
Overexposure	Likelihood	U	2	U	3	U	3	U	2	U	3
	Severity	L		L		L		L		ML	
Air Contaminants	Likelihood	U	3	U	2	MU	3	MU	3	U	2
	Severity	ML		L		L		L		L	
Total		14		23		18		14		15	

All sensors perform much better in a residential application than commercial/industrial. The IR sensor scored the lowest for both commercial/industrial

and residential applications, largely due to having no issue with false triggering gases. The EC sensor scored the highest in both, showing a poor response to both false triggering and poisoning gases. The catalytic-type sensor demonstrated the second best overall score. Poisoning gases in both applications and overexposure in commercial/industrial applications showed to be the biggest issue. The heated diode and MOS sensors fell somewhere in the middle. For the heated diode sensor, humidity was a large issue in the commercial/industrial application, yet poisoning gases were not an applicable failure mode for it. Finally, the MOS sensor did not score well in the commercial/industrial application, but there were no major concerns in the residential application.

After reviewing and comparing the technologies, Wagner and Ferenchaick [2] concluded that three of the available technologies were not practical for A2L refrigerant detection and integration into existing HVAC equipment for commercial/industrial and residential applications. EC sensors were anticipated to be the most likely to fail in both applications. Additionally, the industry does not consider this technology practical for sensing fluorinated refrigerants. Although catalytic-type sensors showed the second lowest susceptibility to failure, they are not considered a viable technology for detecting A2L refrigerants. In detection of fluorinated refrigerants, the byproducts formed by combustion would poison the sensor. Sensor manufacturers were not aware of any efforts to utilize heated diode technology to detect A2L refrigerants in stationary systems. Additionally, rankings from Tables 1.4 and 1.5 indicate adaption into such a system would be difficult [2].

IR sensors appear to be the most practical choice for the commercial/industrial application. They are already widely used, and any sort of maintenance is less of a concern because commercial/industrial equipment are regularly serviced. However, they are very expensive, ranging from \$1,000 to \$12,000 for a stationary system. MOS sensors are also a viable option for this application if placed in a clean area, but they are a better fit for the residential application according to their rankings. They are commercially available at much lower prices; just the sensing element itself is obtainable for as low as \$3. However, the susceptibility to contamination and interference from other gases still remains an issue [2].

Danfoss is a leader in gas sensors for refrigerants. Their application guide [3] discusses the four technologies they market: MOS, EC, catalytic-type, and IR. Table 1.6 summarizes which of the four technologies are suitable to certain refrigerants, according to the guide. A2L refrigerants fall under the category of halocarbons, so two of the four technologies are not suitable for A2L refrigerant detection. EC sensors are

Table 1.6. Suitability to certain refrigerants, reproduced from [3].

	Semi-conductor	Electro-chemical	Catalytic	Infrared
Ammonia "low" concentration (< 100 ppm)	-	✓	-	-
Ammonia "medium" concentration (< 1000 ppm) ¹⁾	(✓)	✓	-	(✓)
Ammonia "high" concentration (<10000 ppm)	✓	-	✓	(✓)
Ammonia "very high" concentration (> 10000 ppm)	-	-	✓	(✓)
Carbon Dioxide CO ₂	-	-	-	✓
HC Hydrocarbons	(✓)	-	✓	(✓)
HCFC - HFC Halocarbons	✓	-	-	(✓)

 Best solution

 Suitable - but less attractive

 Not suitable

only suitable for ammonia, and catalytic-type sensors are not suitable due to poisoning. MOS sensors are the best option, followed by IR sensors. However, their IR sensors are the most expensive sensors they market [3].

1.3.1.1 Selection of Sensing Technology

After careful consideration, it was determined that the MOS sensor was the most sensible technology to pursue. Although infrared sensors were a close second option, they are simply too expensive currently for residential applications. MOS sensors are inexpensive, long-lasting, and already widely used. Although poisoning and interference from other gases remains a possibility, further testing will help characterize MOS sensors to such gases. Not much work has been done on MOS sensor response time to specifically A2L refrigerants, but testing will confirm whether or not a response to 100% LFL in under 10 s can be confirmed.

1.3.2 Introduction to MOS Technology

MOS sensors [6] [7] [17-18] are widely used today in a variety of industries for their gas detection capability. This is largely due to the suitability of many metal oxides for detecting gases by conductive measurements [7]. However, the actual underlying mechanisms that create a response from the gas have been a subject of study for some time.

There are a number of metal oxides suitable for gas detection because of their conduction, although the most common is SnO₂. Due to the wide variety, metal oxides were divided into two groups based on their electronic structure: transition-metal

oxides and non-transition-metal oxides. Non-transition-metal oxides include pre-transition-metal oxides and post-transition-metal oxides [17]. Transition-metal oxides have multiple oxidation states, so they are more sensitive to the environment because the oxidation state can increase or decrease depending on the oxide. However, their instability in structure limits their application in the field. Non-transition-metal oxides only have one oxidation state [18]. There are two specific electronic structures found in metal oxides that are useful for gas sensing: the d^0 structure is found in transition-metal oxides, and the d^{10} structure is found in post-transition-metal oxides [7]. Pre-transition-metal oxides are not often used in gas sensing due to difficulties encountered in electrical conductivity measurements. They are expected to be inert due to their large band gap [17].

Understanding band theory is important to describing how MOS technology works. The main principle of band theory is that within each lattice, a valence band and conduction band are separated by varying amounts of energy. This energy level, or the Fermi level, is defined as the energy level right above where the probability of finding an electron is zero at a temperature. As shown in Figure 1.1, there are three different main materials in band theory: insulators, semiconductors, and conductors [6].

In insulators, too much energy is required to push the electron from the valence band to the conduction band, so electronic conduction does not occur. In a semiconductor, the gap is much smaller. However, there is still a Fermi level where at energies below it, conduction does not occur, and only begins to occur at energies

above it. In conductors, the Fermi level exists within the conduction band, so essentially conduction always occurs [6].

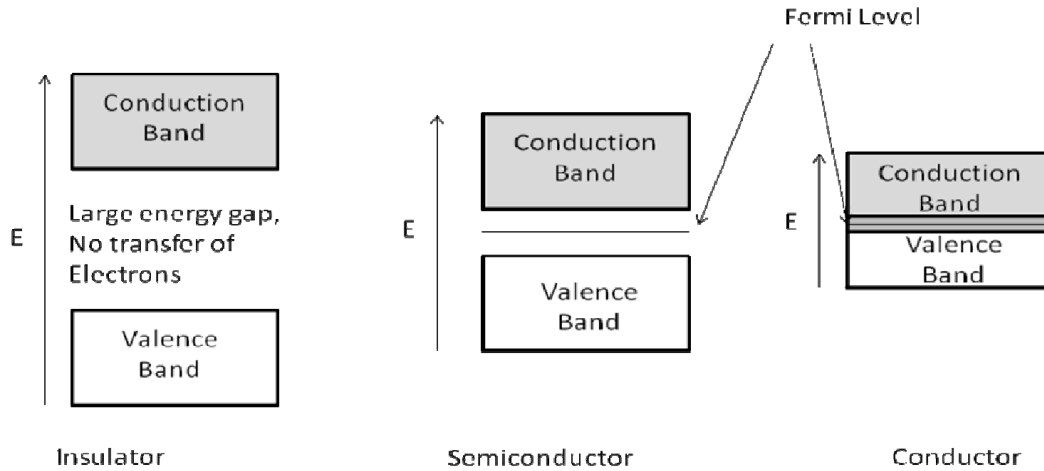


Figure 1.1. Schematic band diagrams of an insulator, semiconductor, and conductor. Reproduced from [6].

The band theory can be applied to MOS sensors. From the target gas, molecules are adsorbed on the surface of the metal oxide film and interact with O^- distributed along the surface. This pulls electrons from the conduction band to the surface to create charged molecules. As shown in Figure 1.2, where O_2 is the target gas, these charged molecules cause the conduction and valence bands to bend upwards and thus reduce the conductivity [7]. E_V , E_F , and E_C represent the valence band, Fermi level, and conduction band. $eV_{surface}$ represents the potential barrier. λ_{air} represents the electron-depleted region that results from electrons being pulled to the surface; the thickness is the length of the band bending region.

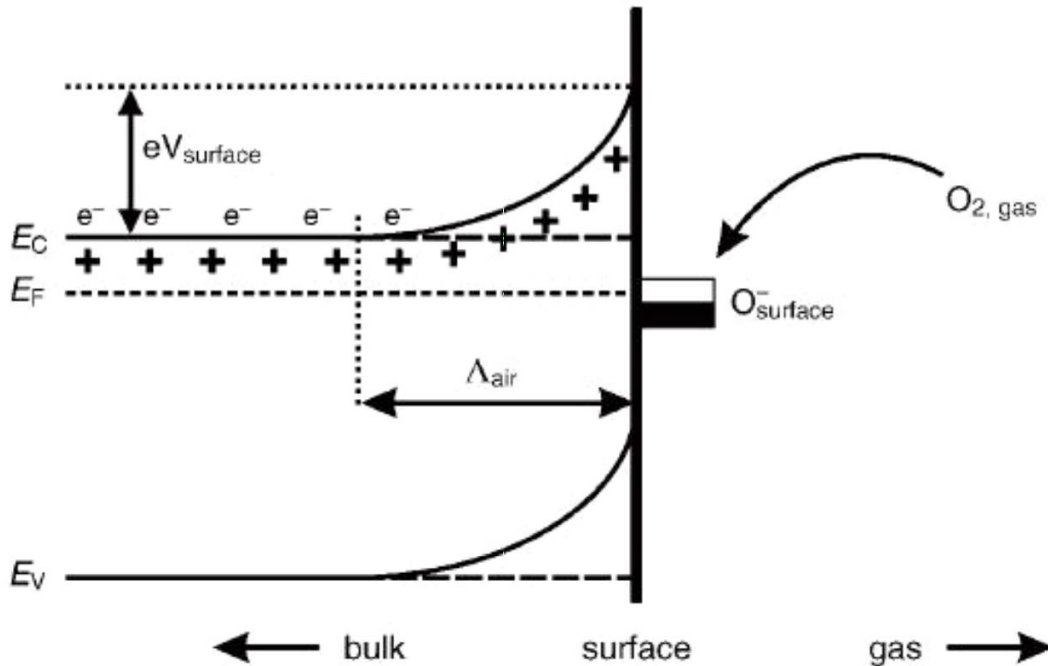


Figure 1.2. Schematic diagram of band bending. Reproduced from [7].

The ideal operating temperature for most MOS sensors is 300-450°C because this is where O^- absorption is the dominate surface activation mechanism [7]. Figure 1.2 only applies to n-type semiconductors, where the majority charge carriers are electrons. In p-type semiconductors, the process is the same except that positive holes are the majority charge carriers, so the effects are reversed. For example, in a case where O_2 is the target gas, the conduction would increase as opposed to decreasing [6].

1.3.3 Comparison of Available MOS Sensors

There are a number of different MOS sensors available on the market, all of which differ in price, size, and capability. Figaro presents an MOS refrigerant gas sensor module shown in Figure 1.3(a) [4] with the model number FCM2630-C00. According

to the specifications [4], this sensor targets and is pre-calibrated to R-32, detects in the range from 1,000 to 10,000 ppm, and consumes 0.3 W. It delivers an analog output and costs US \$47.40. This sensor module uses the gas sensor TGS2630. Figaro offers two other gas sensors that could potentially be integrated with the sensor module. TGS3830 targets halocarbon gases but only in the range of 5-100 ppm, which is much lower than what is required. TGS832-F01 is another sensor possibility, but it consumes three times the power of TGS2630. It is also only available as a gas sensor and would have to manually be integrated into the sensing module.

Mikroe offers an MOS gas sensor module shown in Figure 1.3(b) [8] called MIKROE-1630 which uses the MQ-135 gas sensor. According to the specifications [8], it is Arduino capable and comes with the required code, which makes it easy to connect to a computer. It is also available for US \$16.50, which is nearly three times cheaper than the Figaro FCM2630-C00. However, it must be manually calibrated, and the target gases do not include halocarbon refrigerants. It also requires 0.8 W for power.

SGX offers an MOS gas sensor called MiCS-5524 that Adafruit has attached to a small smartboard, shown in Figure 1.3(c), and sells for as cheap as US \$13.75. However, it is not specified for refrigerant gases, but rather indoor carbon monoxide and natural gas leaks upwards of 1,000 ppm according to the specification sheet [9]. It would require soldering to an analog connection, as well as manual calibration.

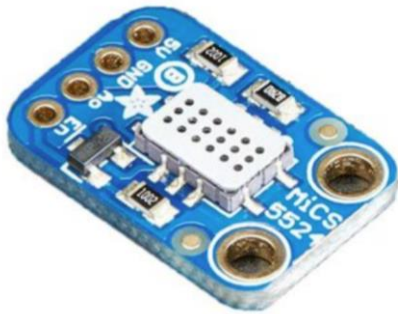
Honeywell carries a large MOS sensor shown in Figure 1.3(d) called the Manning VL. Although it is listed to detect refrigerant fluids [10], it is only available at \$1,174. Its cost and size exclude this sensor from being a viable option.



(a) Figaro FCM2630-C00 [4]



(b) Mikroe MIKROE-1630 [8]



(c) Adafruit MiCS5524 [9]



(d) Honeywell Manning VL [10]

Figure 1.3. Commercially available MOS sensors, reproduced from [4], [8-10].

1.3.3.1 Selection of Sensor

The Figaro FCM2630-C00 refrigerant gas sensor module is the clear MOS sensor option to pursue and acquire. The detection range is the largest available which will leave plenty of room for testing varying concentrations. The fact that it targets and is pre-calibrated to a halocarbon gas gives it a significant boost over the other sensors.

Although it is more expensive than a few other options, it is still very affordable at less than \$50. There are also other sensor options that are Arduino compatible which are more attractive than an analog connection because they can directly connect to a computer. However, this is a minor detail when considering how well the Figaro sensor module fits to the research goals of this thesis. Multiple Figaro FCM2630-C00 sensor modules will be acquired for testing.

Chapter 2: Experimental

2.1 Sensor Specifications

The Figaro FCM2630-C00 is “an embedded type module using the semiconductor gas sensor TGS2630 which is optimized to detect A2L refrigerant gas R-32” [4]. The integrated module eliminates the need for the user to manually construct a circuit to operate the sensor. The sensor itself has a built-in filter to reduce the interfering effects of other gases, which results in a higher selectivity towards R-32. The sensor’s

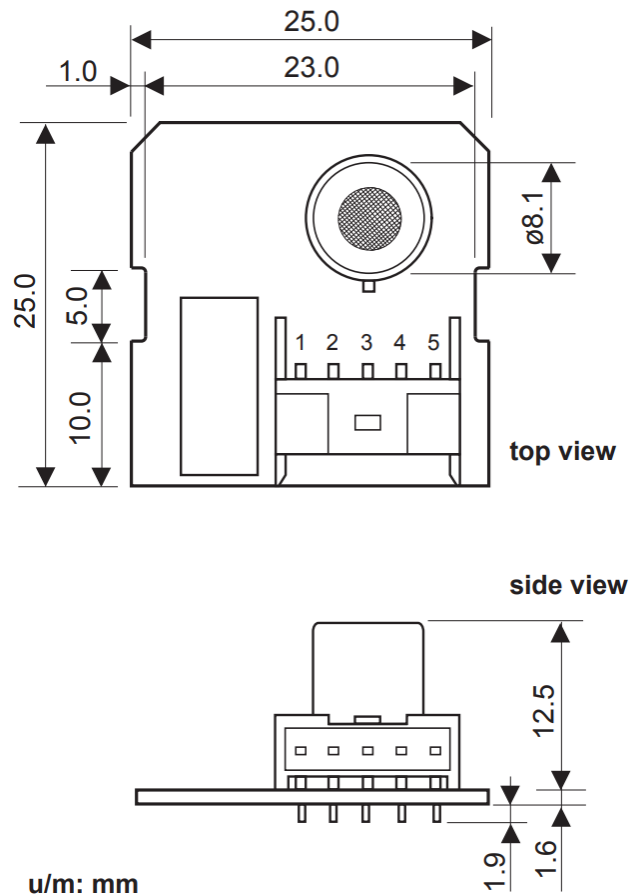


Figure 2.1. FCM2630-C00 structure and dimensions, reproduced from [4].

dimensions are 25x25x17 mm, and it weighs about 4 g. Figure 2.1 shows the structure and dimensions of the sensor module [4].

On the top view, there are numbers labelled 1-5 directly below the sensor. These numbers represent the pin connections on a replaceable connect that allows for periodic maintenance; the pin connections are given by Table 2.1 [4].

Table 2.1. FCM2630-C00 pin connections, reproduced from [4].

Pin No.	Name	Description
1	V _c	Circuit voltage
2	V _{out}	Output voltage
3	V _{REF}	Reference voltage
4	-	-
5	GND	Common ground

Pins 1 and 5 are inputs, and pins 2 and 3 are outputs. The circuit voltage, V_c , is kept at 5.0 ± 2.0 V. The output voltage, V_{out} , delivers the actual reading of the sensor depending on the concentration of the refrigerant. The reference voltage, V_{ref} , is the pre-calibrated voltage of the sensor in 5000 ppm R-32. Pin 5 keeps the sensor module grounded [4].

One of the actual sensors acquired from Figaro can be seen in Figure 2.2. Per Table 2.1, wires are connected to pins 1, 2, 3, and 5, while pin 4 was left open. Because multiple sensor modules were acquired, a labelling system was needed to keep track of which and how many tests each sensor was exposed to; this particular sensor was

labelled A5. To obtain data, the sensor module wires must be connected to a data acquisition system (DAQ), as well as a power source.

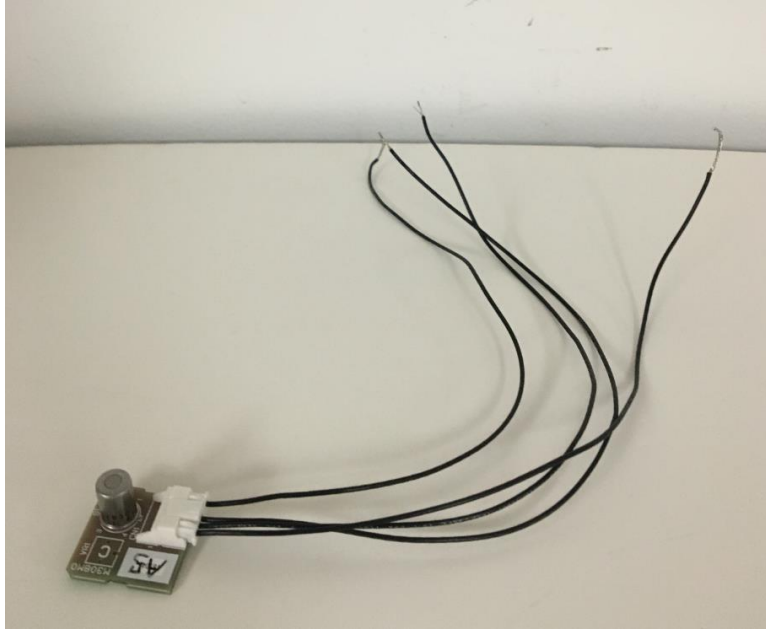


Figure 2.2. Actual FCM2630-C00 sensor module with connected wires.

2.2 Sensor Setup

The components required for the sensor to actually output data were a power supply, positive and negative terminals, and a DAQ. The power supply available was a Tenma 72-13610 bench power supply, and was used to supply power to the DAQ as well as provide a fixed 5 V to both the power and ground terminals. The power and ground terminals were then connected via analog to the DAQ. The DAQ acquired was from National Instruments, and had both a digital component and analog component to it. Only the analog side was used. To connect the sensor, pin 1 was connected to the power terminal. Pins 2 and 3 were connected to the DAQ as analog inputs, and pin 5 was

connected to the ground terminal. There is also a switch that is connected to both the power supply and the DAQ that is manually flipped to indicate the sensor has been plunged into the refrigerant. All wire ends were firmly pressed into the connection piece, and were tightly wound around it when possible, to ensure smooth connections and reduce any potential interfering noise. Figure 2.3 displays the component and wire arrangement, and Figure 2.4 shows a simplified schematic for better understanding.

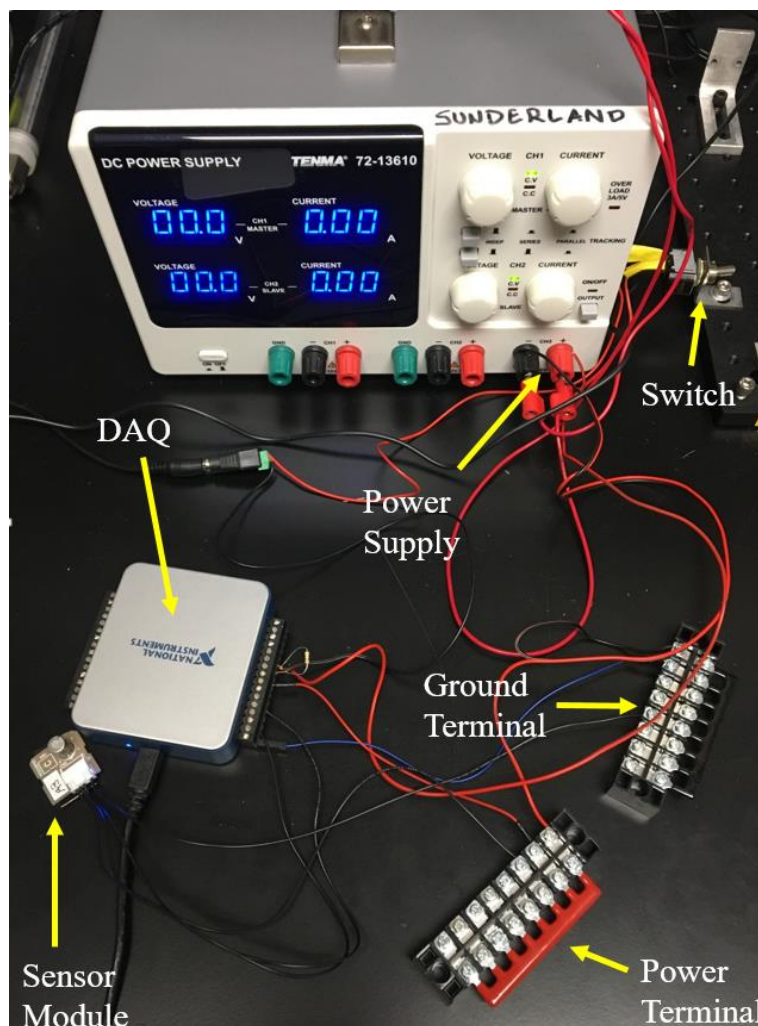


Figure 2.3. Wiring arrangement.

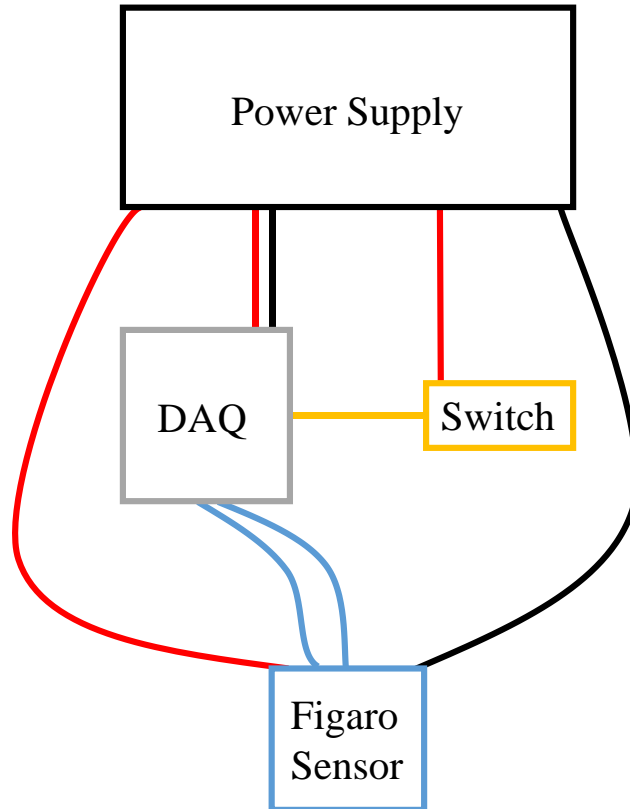


Figure 2.4. Wiring schematic.

To actually observe voltage changes and interpret data, the DAQ is connected by USB to a computer. Among other software applications, LabVIEW was one of the suggested applications to configure measurements. This software provided a clean interface to observe real time voltage fluctuations from the sensor module. Figure 2.5 shows the computer display from the user's point of view. This voltage output is a result of the sensor sitting in ambient air, as seen in Figure 2.3. To start the test, the DAQ was connected to the computer, the desired filename and save path was entered, and the start button was clicked. To stop the test, the stop button was simply clicked and the application was closed; the file is automatically saved to the name and path that was entered.

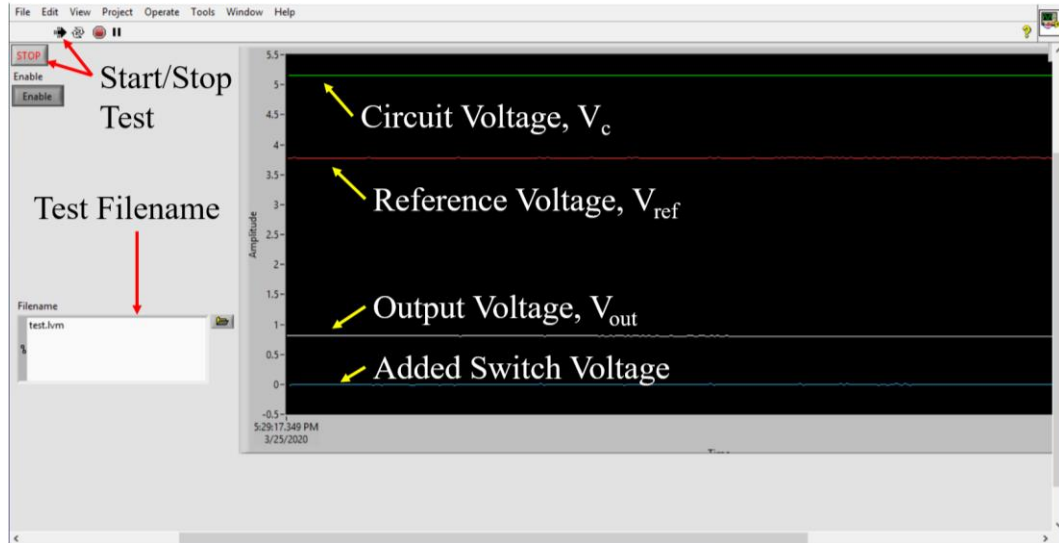


Figure 2.5. LabVIEW user interface.

2.3 Test Apparatus

This section describes the apparatus constructed to flow a mix of air and refrigerant vapor. While the apparatus is essentially the same for flowing contaminants prescribed by UL 60335-2-40, slight modifications were made that are described in Chapter 4. UL 60335-2-40 does not have specific requirements on how the apparatus should be designed, so the apparatus presented here is one of many options. The apparatus is an original concept designed by previous students who contributed to the project, and is not known to be similar to any other apparatuses.

To test the sensor, an apparatus was constructed to deliver a mix of air and the refrigerant at varying concentrations to a sealed test vessel for the sensor module to be plunged into. The apparatus can be seen in Figure 2.6, and a schematic diagram is presented in Figure 2.7. First, two rotameters, one larger than the other, were mounted onto a board; the smaller rotameter was used for refrigerant flow, and the larger

rotameter was used to flow air. For the refrigerant line, PVC flexible tubing was connected from the refrigerant supply to a pressure regulator to control the pressure of the incoming refrigerant. The pressure regulator was connected to a thermometer probe to monitor the incoming temperature of the refrigerant. The thermometer probe was connected to a needle valve to adjust the flow of the refrigerant accordingly. The needle valve was connected to the inlet of the rotameter which displayed a flowrate corresponding to the height of the tracking ball within it. The pressure gauge, thermometer probe, and needle valve are all mounted on the same board as the rotameter.

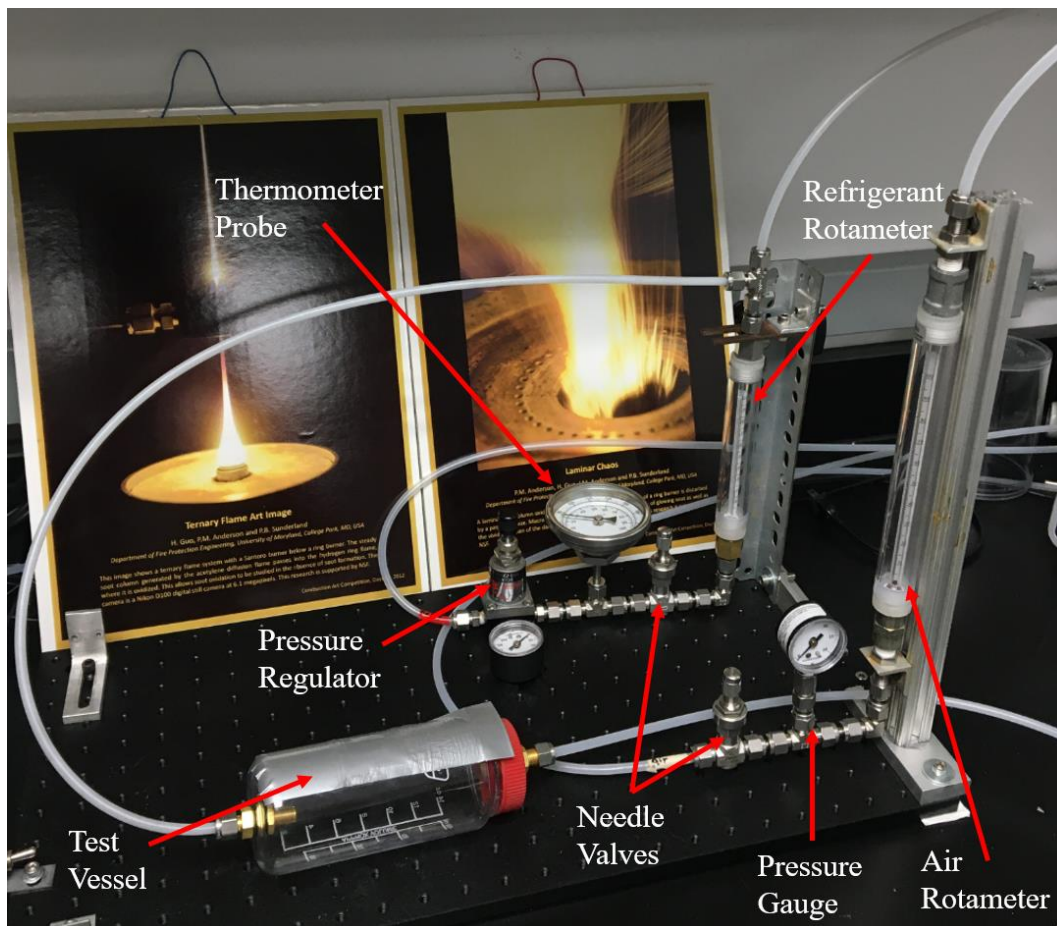


Figure 2.6. Test apparatus.

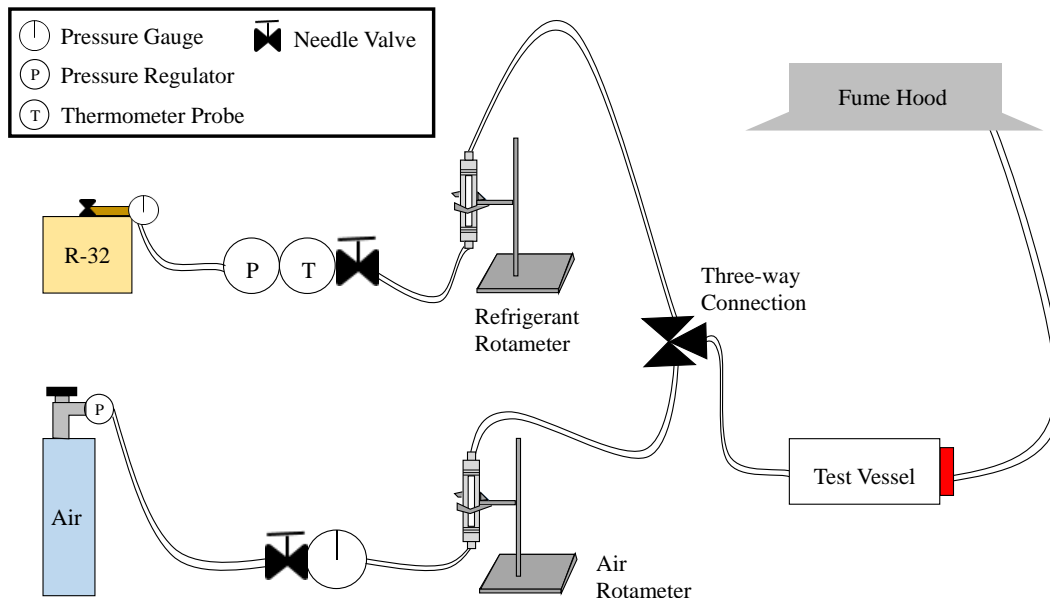


Figure 2.7. Test apparatus schematic.

For the air line, the same PVC tubing was connected from an available shop air supply to a pressure gauge and needle valve assembly that connected to the rotameter inlet for air flow, which were all mounted on the same board as well. Tubing that is connected to the outlet at the top each rotameter then meets at a tee connection to allow the gases to mix after they flow through their respective rotameters. Tubing extends from the outlet of the tee connection to the inlet of the test vessel, where the gases can mix into equilibrium. Tubing then extends from the outlet of the test vessel to a fume hood for exhaust so that there is minimal gas presence outside of the actual apparatus.

The test vessel, shown in Figure 2.8, is a standard 500 mL Nalgene bottle. A hole was drilled in the center of it measuring the diameter of the sensing tip found in Figure 2.1. Only the sensor was plunged into the vessel as opposed to the whole sensor module to minimize the exposed surface area. Two more holes were drilled on the top

and bottom of the vessel for the tube fittings. The vessel was fit with a duct tape cover. The duct tape cover typically lays flat across the vessel to keep it sealed, and is only pulled back to plunge the sensor into the vessel.

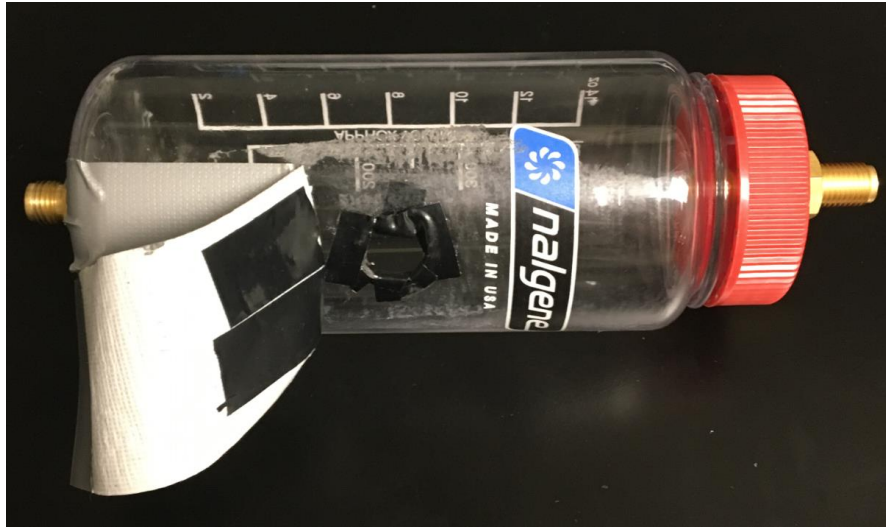
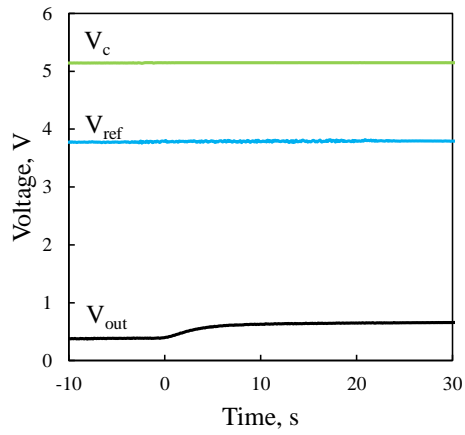


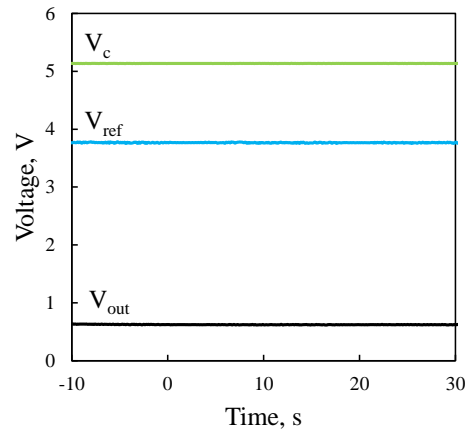
Figure 2.8. Nalgene 500 mL vessel.

2.4 Effect of Humidity

During testing, it was noticed that drier air had an effect on the output of the sensor. When the sensor was plunged with just airflow, V_{out} was observed to increase by about 0.3 V as shown in Figure 2.9(a). The sensor was then tested with increased humidity. The air was bubbled with water to obtain saturated vapor at 95% relative humidity (RH). Figure 2.9(b) shows the sensor's response to just airflow at 95% RH. There is no voltage increase, which is what should be expected; the air used to mix with the refrigerant should produce the same sensor response as ambient air. If air at 0% RH was used for further testing, the voltage increase it produces would interfere with the sensor's response to other gases.



(a) 0% RH



(b) 95% RH

Figure 2.9. Effect of humidity.

To obtain air at 95% RH, a filtering flask assembly was used as seen in Figure 2.10. A hole of the diameter of the glass dispersion tube was drilled through a black



Figure 2.10. Filtering flask assembly.

rubber stopper, and the dispersion tube was fit through it. Tubing was fit on top of it with a fitting on the other end to connect to the top of the rotameter for air. The 500 mL filtering flask was filled with distilled water, and the tube was placed in the water with the dispersion tip submerged. The flask was sealed with the rubber stopper. Tubing was then slipped onto the arm of the flask and connected to the connection tee. Air at 95% RH was used for the extent of testing.

2.5 Soap Bubble Calibration

To obtain the correct concentrations required from the various tests, accurate flowrates are required to determine how much air dilution is needed. Different refrigerants and other gases will yield different flowrates, so multiple calibrations need to be done. The ball height on the rotameters corresponds to a number, but unfortunately the flowrates are not marked, and there will be different flowrates from different gases anyways. Therefore, it is crucial to establish a calibration method. A method using a soap bubble meter was found to yield accurate results, and was used throughout the course of testing.

Soap bubble flowmeters are long glass tubes with volumetric measurement values along the side. They are open at the top, and have an opening for incoming flow near the bottom. On the very bottom is a rubber pipet bulb containing a soap solution. With incoming flow, the rubber pipet bulb would be squeezed to form a soap bubble that would travel up the flowmeter. A volumetric flowrate can be determined from the volume the soap bubble covers in a certain amount of time.

The soap bubble flowmeters used for calibration can be seen in Figure 2.11. The smaller soap bubble flowmeter was 10 mL and was used to calibrate the refrigerant rotameter. The larger soap bubble flowmeter was 100 mL and was used to calibrate the air rotameter because the flows were faster. For calibration, the desired soap bubble flowmeter was connected to the top of the desired rotameter, and the gas was flowed. Using the needle valves, the flow was adjusted until the bottom of the tracking ball was at a height of 10 on the rotameter. A soap bubble was then created in the soap bubble flowmeter by squeezing the pipet, and a timing device was used to track how long it took for the soap bubble to travel a certain volume up the flowmeter. The volumetric



Figure 2.11. Soap bubble flowmeters.

flowrate was recorded, and the process was repeated. An average between two flowrates was obtained at increasing ball height intervals of 10 on the rotameter all the way up to 100 for a total of 10 calibrated flowrates.

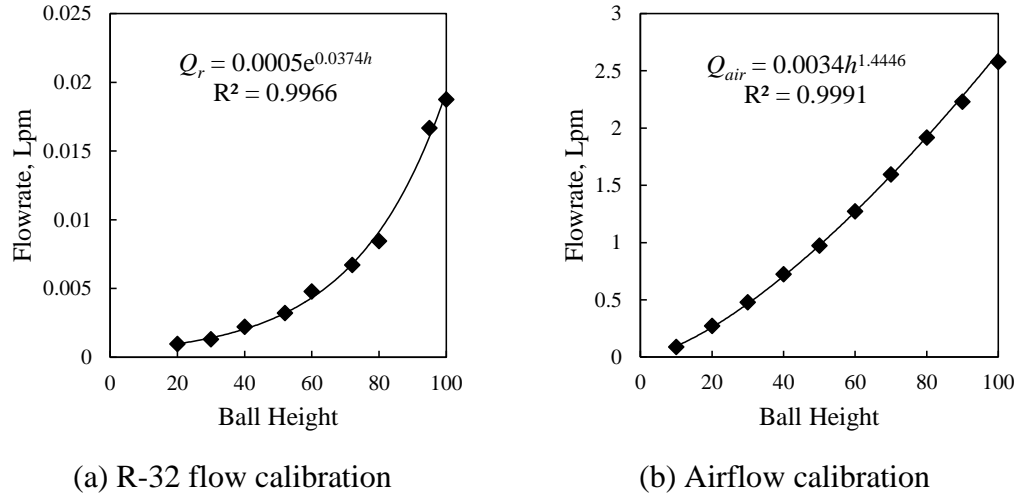


Figure 2.12. Calibrated flowrates as a function of ball height.

The flowrates are converted to units of Lpm. These points can be plotted on a graph and fit with a trend line to show the flowrate as a function of the ball height. Figure 2.12(a) shows the relationship between the ball height, h , and flowrate for R-32 flow, Q_r , on the smaller rotameter. Figure 2.12(b) shows the relationship for the air flowrate, Q_{air} , on the larger rotameter. The ball height-flowrate relationship for R-32 represents an exponential relationship, while the air flow calibration plot appears much more linear. The flowrate can now be determined from any ball height using the trend line equations. The desired percent of the LFL, $LFL\%$, can then be reached by

$$LFL\% = \{100[Q_r/(Q_{air} + Q_r)]\}/LFL, \quad (2.1)$$

The LFLs for R-32 and R-454B are 14% [19] and 11.25% [20]. The smaller rotameter was of course re-calibrated for R-454B to obtain a different equation for Q_7 . This calibration method allows for the flowrates of the refrigerant and air to be adjusted so that varying percentages of the LFL can be reached while remaining precise.

Chapter 3: Response to Refrigerant Leaks

3.1 Plunge Tests

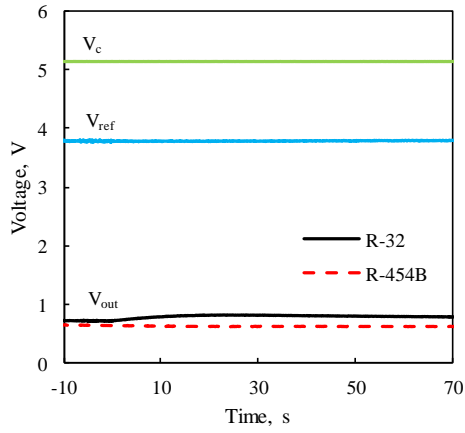
Testing for the response time of the MOS sensors is extremely important to observe how quickly MOS sensors respond to dangerous concentrations of refrigerants. When the sensor was factory calibrated, the alarm set-point was set to 5000 ppm R-32. The reference voltage, V_{ref} , indicates the factory calibrated alarm set-point; the intention was for the sensor to be in a monitoring state if the sensor output voltage, V_{out} , was less than V_{ref} , and an alarm state if V_{out} was greater than V_{ref} [4]. However, recent updates to UL 60335-2-40 require the leak detection system to activate at 25% LFL of the refrigerant. Additionally, the sensor is required to trigger an alarm within 10 s to refrigerant exposure according to Annex LL, Section 3 of UL 60335-2-40. The response time is determined by immersing the sensor in 100% LFL of the refrigerant and measuring the time for V_{out} to reach the alarm set-point of 25% LFL [5]. This procedure first requires calibrating the sensor response to a concentration of 25% LFL to determine the V_{out} at the alarm set-points. Obtaining the sensor's response voltage in response to a concentration of refrigerant is done through a plunge test.

For a plunge test, refrigerant and air were allowed to flow into the vessel. The flowmeter for each gas was adjusted to obtain the desired LFL concentration for the refrigerant. The mixture was allowed to run for 10 minutes to reach equilibrium. The data logger started recording data, and ten seconds of data of the sensor in air were allowed to record. The sensor was then plunged into the vessel, and the switch was flipped to identify time zero. The sensor was plunged by pulling back the duct tape

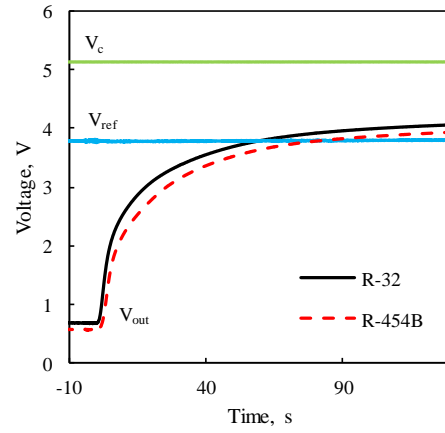
cover, placing the sensor in the pre-drilled hole, then quickly pulling the tape back over to cover the sensor. The sensor was allowed to take data until V_{out} plateaued. The sensor was then removed from the apparatus and left in ambient air.

Although the sensor only needed to be calibrated at 25% LFL, plunge tests were conducted at 0, 10, 75, and 100% of the LFL as well to observe how V_{out} changes with varying refrigerant concentrations. The sensor was left in ambient air for 30 minutes between each plunge test to allow it to fully recover before the next test. Following the plunge tests with increasing concentration steps, the procedure was then repeated starting at 100% LFL and ending at 0% LFL to check for hysteresis. Two sensors were used for a total of four tests at each concentration. Plunge tests were conducted in both R-32 and R-454B.

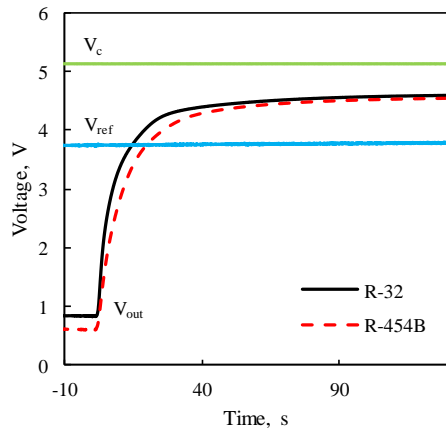
Figure 3.1 shows the average V_{out} values over four trials at 0, 10, 25, 75, and 100% of the LFL for R-32 and R-454B. The circuit voltage of the sensor is represented by V_c in the graphs; it is a constant 5.16 V, which is within the sensor specifications of 5.0 ± 2.0 V [4]. The plunge tests for 10 and 25% of the LFL were ran for 120 s after the sensor was plunged because V_{out} took longer to stabilize at lower refrigerant concentrations. As the concentration increased to 75 and 100% LFL, V_{out} responded much quicker and only took 60 s to stabilize. Figure 3.1a shows a baseline reading for the sensor when there is no refrigerant exposure. As expected, the sensor shows no response to being plunged in pure air. In Figure 3.1b, V_{out} increases quickly in response to refrigerant exposure, then slowly starts to plateau at about 4 V. As the concentrations increase, the V_{out} curve becomes steeper as well in the seconds immediately following initial exposure, indicating quicker sensor response with increasing concentrations.



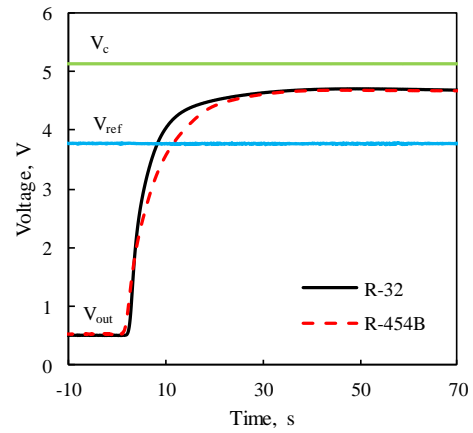
(a) 0% LFL



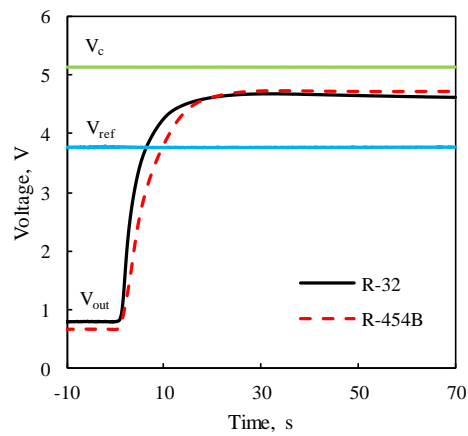
(b) 10% LFL



(c) 25% LFL



(d) 75% LFL



(e) 100% LFL

Figure 3.1. Sensor response to increasing refrigerant concentration steps at (a) 0% LFL, (b) 10% LFL, (c) 25% LFL, (d) 75% LFL, and (e) 100% LFL.

V_{out} also reaches a higher voltage value before beginning to plateau with each increasing LFL percentage step. For each plunge test, the R-454B curve is slightly below the curve for R-32, demonstrating that the sensor takes longer to respond to R-454B than R-32 for the same refrigerant concentration.

Table 3.1 shows the average values of the voltage difference for each discrete concentration. The voltage difference was calculated using

$$\Delta V = V_{out} - V_{ref}. \quad (3.1)$$

Although V_{ref} no longer represents the alarm set-point, this convention is still used because V_{ref} is indicative of the temperature near the gas sensor module [4], and drifts in accordance for each test by ± 0.05 V [4]. V_{ref} was observed to read approximately 3.8 V.

Table 3.1 Voltage differences at various concentrations of refrigerant, V.

	0% LFL	10% LFL	25% LFL	75% LFL	100% LFL
R-32	-3.20	0.217	0.782	0.875	0.915
R-454B	-3.14	0.0909	0.739	0.885	0.943

It is interesting to note that when the sensors are plunged in only air, the sensor is still outputting a signal. A voltage difference of -3.8 V at 0% LFL would indicate the sensor is not detecting any refrigerant leak, but the results show that V_{out} is instead reading about 0.6 V. At a concentration of 10% LFL, ΔV for R-32 is slightly higher than that of R-454B. This is likely due to R-32 having a higher LFL at 14% by volume, compared to the LFL for R-454B of 11.25% [19-20]. Therefore, the sensor is detecting a higher concentration of R-32 than R-454B at the 10% LFL, so V_{out} is reading a higher steady-state voltage. This explains why the R-454B curve is consistently slightly below

the R-32 curve in Figure 3.1. Additionally, ΔV has become positive at the 10% LFL, indicating that the steady-state V_{out} is greater than V_{ref} . This shows that the factory calibrated alarm set-point is below the 10% LFL of the refrigerant, indicating a safety factor of over 10 to ensure flammable concentrations are not reached at 100% LFL. Although the approach is cautious, an alarm set-point at 25% LFL would trigger fewer alarms while still providing a safety factor of 4.

The voltage difference at 25% LFL is the most significant finding because this voltage will be used to characterize response time. As expected, ΔV values at 25% LFL are slightly higher than those at 10% LFL. The voltage difference value for R-32 is higher than the value for R-454B, which is consistent with the 10% LFL results. At 75 and 100% LFL, the voltage difference values continue to increase slightly, but begin to converge as higher concentrations are reached.

Figure 3.2 shows the logarithmic relationship between the steady-state output of the sensor and concentration of the refrigerant. There is a large increase from the steady-state V_{out} at 0% to 10% LFL, followed by smaller increases in voltage differences to 100% LFL. The data again shows smaller ΔV values for R-454B than R-32 at 10 and 25% LFL, but very similar values at 75 and 100% LFL. The data was fit with a logarithmic trendline that indicates a nearly identical relationship between the sensor's response to R-32 and R-454B exposure at various LFL concentrations. Figure 3.3 shows the same data plotted with a logarithmic scale on the x-axis. The R^2 values for both refrigerants are above 0.99 which reinforces the strength of the logarithmic relationship.

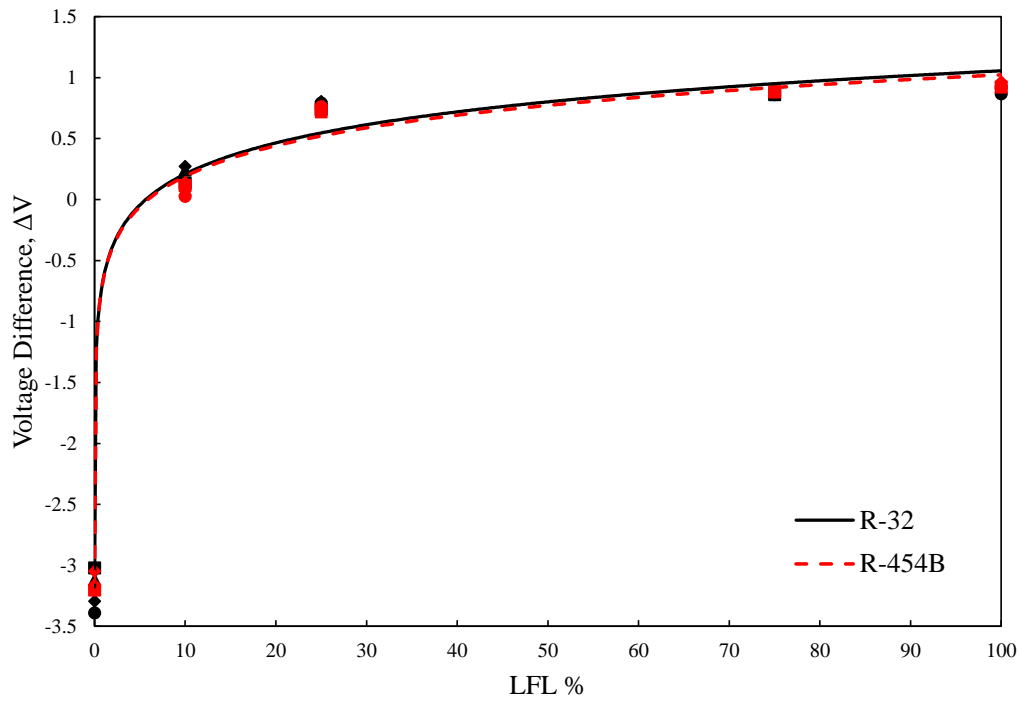


Figure 3.2. Voltage difference for various concentrations of R-32.

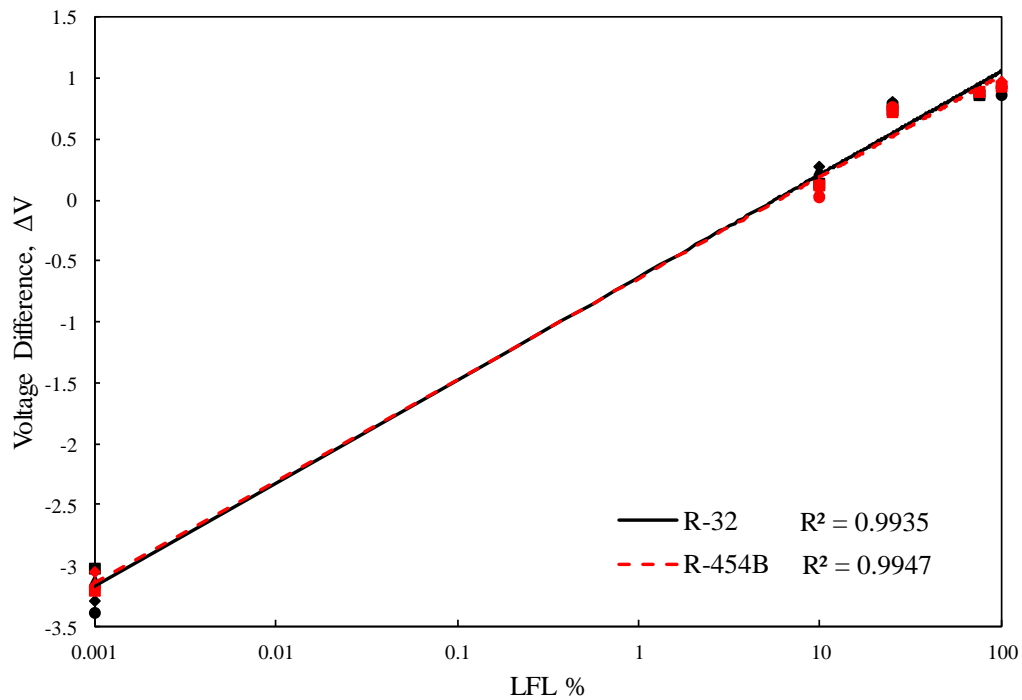


Figure 3.3. Voltage difference for various concentrations of R-32 on a logarithmic scale.

3.2 Response Time Tests

After obtaining the sensor's response to a concentration of 25% LFL, the response time of the sensor can be determined by plunging the sensor into 100% LFL of the desired refrigerant, per Annex LL, Section 3 of UL 60335-2-40 [5]. The response time test procedure is similar to that of the plunge test, except the sensor is only plunged in 100% LFL. Where V_{out} crosses the 25% LFL steady-state output voltage, which was determined by the plunge tests, is considered the response time of the sensor.

Table 3.2 displays the response time to the 25% LFL for each of the four tests. The data for the second test of R-32 was not used because the duct tape cover was not sealed properly, thus exposing the sensor to more ambient air which drastically increased the response time. The data for one sensor is represented in tests 1 and 3, while the data for the other sensor is represented in tests 2 and 4. The response time in the first test for R-32 is noticeably slower than the response time in other tests; one explanation is that the refrigerant and air mixture did not reach a full equilibrium before the sensor was plunged, so the concentration in the test vessel could have been slightly less than the 100% LFL.

There seems to be no distinguishable pattern in the data between the two sensors, or between the first and second response time test for each sensor. It should be noted that all the response times are greater than 10 s, which does not satisfy the requirements of UL 60335-2-40. The average response times at the 25% LFL for R-32 and R454-B were 18.8 s and 16.8 s, respectively.

Table 3.2. Sensor response time to 25% LFL, s.

	Test 1	Test 2	Test 3	Test 4
R-32	29.1	--	12.1	15.1
R-454B	14.1	19.5	15.4	18.0

Although the response time test data for the 25% LFL does not satisfy the 10 s requirement, the time for the sensor output voltage to reach 10% LFL can be observed from the same response time tests, and is displayed in Table 3.3. The average response times at the 10% LFL for R-32 and R454-B were 8.03 s and 10.5 s, which satisfy the 10 s response time requirement, although R-454B is just slightly above.

Table 3.3. Sensor response time to 10% LFL, s.

	Test 1	Test 2	Test 3	Test 4
R-32	10.4	--	7.1	6.6
R-454B	8.5	12.1	9.6	11.7

Figures 3.4 and 3.5 show the sensor's response to 100% LFL for R-32 and R-454B, which was averaged across the four tests. The 10 and 25% LFL steady-state V_{out} for each refrigerant is labelled for reference. The 10 seconds of data collection in air is indicated, then the sensor is plunged at 0 s. V_{out} sharply increases in response to the refrigerant exposure until leveling out after about 25 s. These figures provide a visual representation of V_{out} reaching the 10% LFL steady state voltage before the 25% LFL.

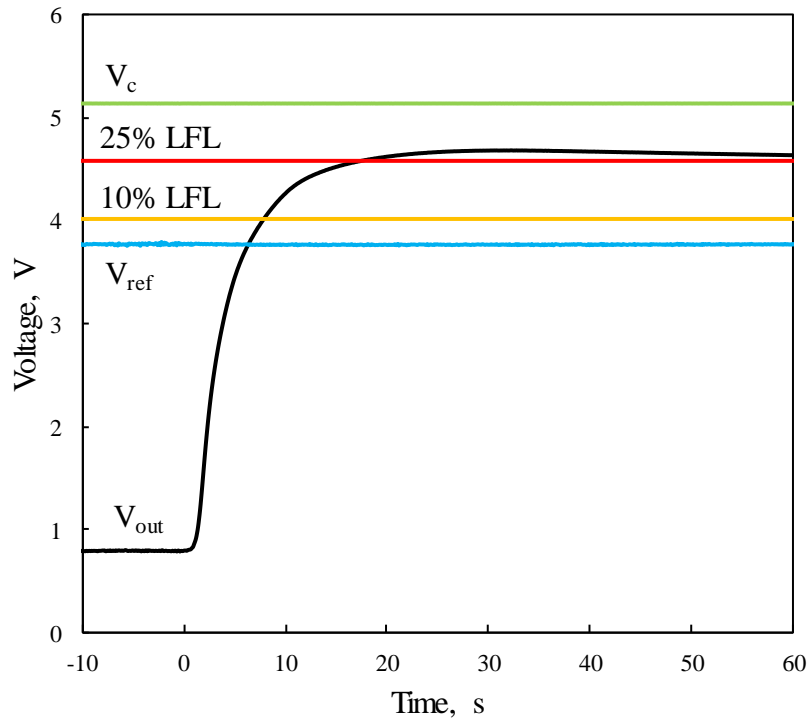


Figure 3.4. Response time test for R-32.

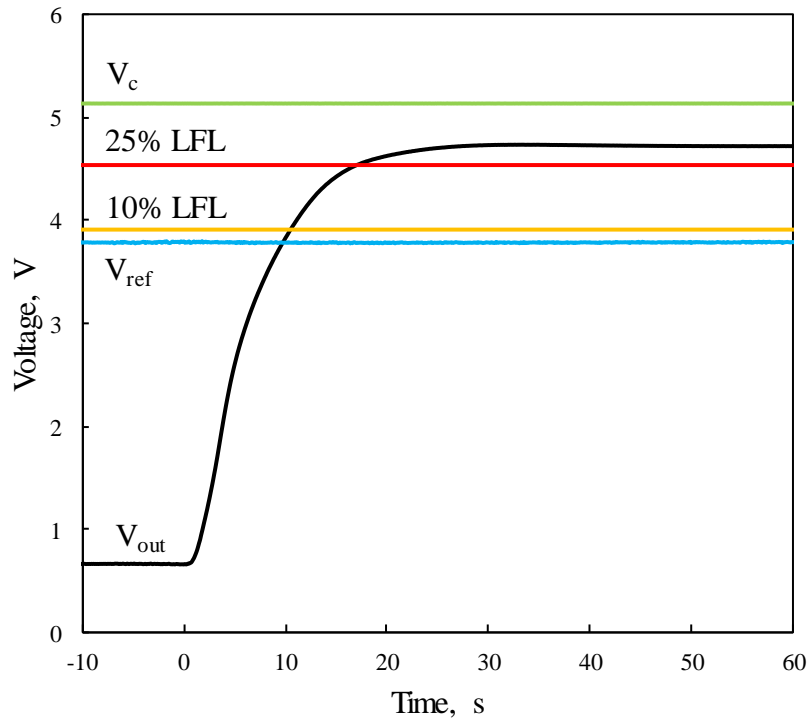


Figure 3.5. Response time test for R-454B.

Although the MOS sensors do not respond to the 25% LFL within 10 s, one solution could be to lower the alarm set-point threshold to the 10% LFL. This could potentially trigger more alarms, but it would satisfy the response time requirement.

Chapter 4: Contaminant Tests

4.1 Contaminant Test Procedure

At any given time during the operation of the sensor, it is likely that it will be exposed to other contaminants besides refrigerant vapor leaks. Contaminants found in common household products such as hairspray, cleaning solutions, and paints could easily make their way into the air surrounding the sensor, and cause the sensor to fail in one of two ways. The first is to cause the sensor to return a false alarm, meaning that the contaminant would raise the sensor's output voltage above the alarm set-point. This would trigger the alarm and indicate the presence of a refrigerant concentration above 25% LFL when there is actually no leak at all. The sensor could also fail by becoming poisoned by the air contaminant. Prolonged exposure to contaminants that the MOS technology is not equipped to handle could overheat the sensor and effectively ruin its ability to detect refrigerant leaks. A poisoned sensor would demonstrate a response time much slower than the typical 17 s found from the response time tests, or no response at all.

UL 60335-2-40 Annex LL prescribes a list of contaminants and associated concentrations, shown in Figure 4.1, which the sensors are required to be exposed to. The standard states that the sensors "shall not indicate presence of refrigerant concentration above the set-point" [5]. It is very possible that small amounts of these contaminants can appear in the air; ethanol, for example, is the intoxicating agent found

in alcohol, and isopropyl alcohol is widely used to treat wounds and for cleaning purposes.

Table 4.1. Contaminants and concentrations required for testing, reproduced from [5].

Substance	Concentration, ppm
Methane	500
n-Butane	300
n-Heptane	500
Ethyl acetate	200
Isopropyl alcohol	200
Carbon dioxide	5000
Ammonia	100
Ethanol	200
Toulene	200
Trichloroethane	200
Acetone	200
Silicone	100

Table 4.2 summarizes the phase and concentration, X , of each of the contaminants. Two different siloxanes were chosen to represent silicone in testing. Decamethylcyclopentasiloxane was chosen because it is present in many personal care products, such as hair-spray and anti-perspirant. Octamethylcyclotetrasiloxane was

Table 4.2. Acquired contaminants.

	Formula	Phase	X
Methane	CH ₄	Gas	1
n-Butane	C ₄ H ₁₀	Gas	0.009
Carbon dioxide	CO ₂	Gas	1
Ammonia	NH ₃	Gas	0.0001
n-Heptane	C ₇ H ₁₆	Liquid	1
Ethyl acetate	C ₄ H ₈ O ₂	Liquid	1
Isopropyl alcohol	C ₃ H ₈ O	Liquid	1
Ethanol	C ₂ H ₅ OH	Liquid	1
Toluene	C ₇ H ₈	Liquid	1
Trichloroethane	C ₂ H ₃ Cl ₃	Liquid	1
Acetone	C ₃ H ₆ O	Liquid	1
Decamethylcyclopentasiloxane	C ₁₀ H ₃₀ O ₅ Si ₅	Liquid	1
Octamethylcyclotetrasiloxane	C ₈ H ₂₄ O ₄ Si ₄	Liquid	1

also chosen for its presence in caulks. Four of the contaminants were acquired as gases, two of which were already diluted with air. The rest of the contaminants were acquired as pure liquids.

A standardized test procedure from UL 60335-2-40 follows this list for exposing sensors to the contaminants. Annex LL, Section 5 states to “ensure that the chamber has been well ventilated with fresh air. Place the refrigerant sensor in operation inside the chamber and allow it to run for 15 ± 5 minutes. Close and seal the chamber to prevent air infiltration. Using a syringe or equivalent device, add the calculated amount of the first substance into the chamber at a rate and in a location such that it is well mixed with the air and does not cause localized high concentrations. Allow the refrigerant sensor to remain in the chamber for 2 hours. During this time the output shall not indicate the presence of refrigerant concentration above the (25% LFL equivalent response). Purge the chamber with clean air to remove all of the test atmosphere. Maintain clean air in the chamber for a recovery time of 16 h or as specified by the manufacturer. In no case shall recovery time exceed 16 h. Reseal the chamber and repeat the test using another substance from (Table 4.2) until the refrigerant sensor has been exposed to all substances. It is not required that exposure to the substances be in any particular order” [5].

During actual testing, the procedure was slightly modified. The sensor first operated in clean air within the vessel for 1 min as opposed to 15 min. The contaminant was then flowed into the vessel at the desired concentration. If V_{out} remained stable and showed no response to the contaminant, the test was stopped after 10 min. If the sensor output voltage began to increase, the test was run until V_{out} completely

plateaued. It was assumed that if the sensor demonstrated no response to the contaminant after the first 10 min, then it would continue to show no response for the remainder of the 2 hours. Similarly, it was assumed that if the sensor did show a response, V_{out} would not fluctuate again after stabilizing, and the test could be stopped.

4.2 State of Health Tests

Annex LL, Section 5 of UL 60335-2-40 states that “at the end of the test the refrigerant sensor shall be tested in compliance with LL.3DV”. Section LL.3DV outlines the response time test carried out previously [5]. In contaminant testing, this procedure is referred to as a state of health test because the purpose is to check if the contaminated sensor successfully responds as quickly to the refrigerant as a healthy sensor.

Another modification made was that a state of health test was conducted following each contaminant test after the sensor had operated in clean air for 1 hour. If the sensor fails to demonstrate the same response time as shown in Figure 3.3 following all the contaminant tests, it is unclear which contaminant, or combination of contaminants, was responsible for poisoning the sensor. A state of health test following each contaminant exposure allows the sensor’s state of health to be constantly monitored. The clean air operating time is cut down to 1 hour as opposed to 16 hours to remain consistent with the shortened contaminant test time. After each state of health test, the sensor operated in clean air for 24 hours before the next contaminant was tested.

4.3 Gas Contaminants

Methane, *n*-butane, carbon dioxide, and ammonia were the four contaminants that were available as gases to test. The same apparatus was used, but the rotameter that was used to flow the refrigerant was instead connected to the gas contaminant supply instead of the refrigerant supply. This rotameter was recalibrated for each of these different contaminants prior to testing using the soap bubble method. After calibrating, it was necessary to determine what ratio of air-to-contaminant mixture was needed to deliver the concentration specified in Table 4.1. The flow rate of both air and contaminant going into the vessel, Q_{tot} , was initially set to 1 Lpm, so the flow rate of the contaminant, Q_{gas} , was determined by

$$Q_{gas} = Q_{tot}(X_{test}/X), \quad (4.1)$$

where X_{test} is the test concentration specified in Table 4.1. The amount of makeup air, Q_{air} , needed was then calculated by

$$Q_{air} = Q_{tot} - Q_{gas} \quad (4.2)$$

Table 4.3 shows the Q_{tot} , Q_{gas} , and Q_{air} values needed to determine the air-to-contaminant ratio for each of the contaminants. Both methane and carbon dioxide were available as 100% pure gases with no dilution, so they required the most makeup air. Q_{tot} for these two contaminants was therefore increased to 2 Lpm so that Q_{gas} was just large enough to be flowed using the available rotameters. Because the *n*-butane was available as a 0.9% butane-air mixture, it needed to be flowed at a 30:1 air-to-

contaminant ratio. The ammonia was available at exactly the concentration set forth in Table 4.1, so no makeup air was needed.

Table 4.3. Gas concentrations and flow rates for determining air-to-contaminant ratio.

	Q_{tot} , Lpm	Q_{gas} , Lpm	Q_{air} , Lpm
Methane	2	0.001	1.99
<i>n</i> -Butane	1	0.033	0.967
Carbon dioxide	2	0.01	1.99
Ammonia	1	1	0

4.4 Liquid Contaminants

The remaining eight contaminants were acquired as liquids. Obtaining vapor from these contaminants at the desired concentration required bubbling with nitrogen using the same 500 mL filtering flask and glass dispersion tube that was used to bubble water for the plunge and response time tests. Although this procedure was not outlined by the UL standard, research proved it to be a viable method. Nitrogen was used as opposed to air for safety reasons to avoid oxygen mixing with the flammable contaminant. The bubbling process first requires obtaining an experimental mass loss rate, \dot{m}_{exp} , of each contaminant using a mass scale. From \dot{m}_{exp} , a flow rate from the vapor, $Q_{vap,exp}$, can then be obtained, which will determine how much makeup air is needed to meet the desired concentration for each contaminant. However, the mass loss rate must be calculated first and compared to \dot{m}_{exp} to verify the accuracy of this method.

The calculated mass loss rate, \dot{m}_{calc} , can be determined by

$$m_{calc} = \rho_i Q_{vap,calc}, \quad (4.3)$$

where ρ_i is the density of the contaminant and $Q_{vap,calc}$ is the calculated flow rate from the contaminant vapor leaving the filtering flask. The contaminant density is determined by the ideal gas law, which is given by

$$\rho_i = (p MW_i)/(R_u T) \quad (4.4)$$

p is the atmospheric pressure, MW_i is the molecular weight of the contaminant, R_u is the universal gas constant, and T is the temperature of the flowed nitrogen, which is assumed to be an ambient temperature of 22°C. The calculated flow rate from the contaminant vapor is given by

$$Q_{vap,calc} = Q_{N_2}(p_{vap}/p), \quad (4.5)$$

where Q_{N_2} is the pre-set flow into the filtering flask and p_{vap}/p is the vapor pressure of the contaminant standardized by the atmospheric pressure. The vapor pressure for each contaminant was given at 20°C. However, vapor pressure fluctuates proportionally to temperature, so the Clausius-Clapeyron equation is used to determine the actual vapor pressure based on the temperature of the contaminant at the time of the test. The expression for p_{vap} is

$$\ln(p_{vap}/p_{vap,init}) = -(\Delta H_{vap}/R_u)[(1/T_{test}) - (1/20)] \quad (4.6)$$

where $p_{vap,init}$ is the vapor pressure of the contaminant at 20°C. ΔH_{vap} is the enthalpy of vaporization of each contaminant at 25°C, and T_{test} is the temperature of the contaminant at the time of the test. The temperature was determined using a thermometer probe positioned at the inlet of the vapor flow to the apparatus.

Figure 4.1 shows the layout of the bubbling apparatus. Distilled water was used to confirm that \dot{m}_{calc} would match up well with an experimental mass loss rate. To obtain \dot{m}_{exp} , 200 mL of distilled water was first poured into the filtering flask and then weighed on the mass scale. The weight of the flask before the bubbling, m_1 , was recorded. The glass dispersion tube, connected to the rotameter used for flowing nitrogen, was then placed in the filtering flask. A rubber stopper was fit around the dispersion tube to firmly seal the top of the filtering flask. Nitrogen was flowed at a Q_{N_2} of 1 Lpm to bubble the water for 60 min. During this time, T_{test} was noted from

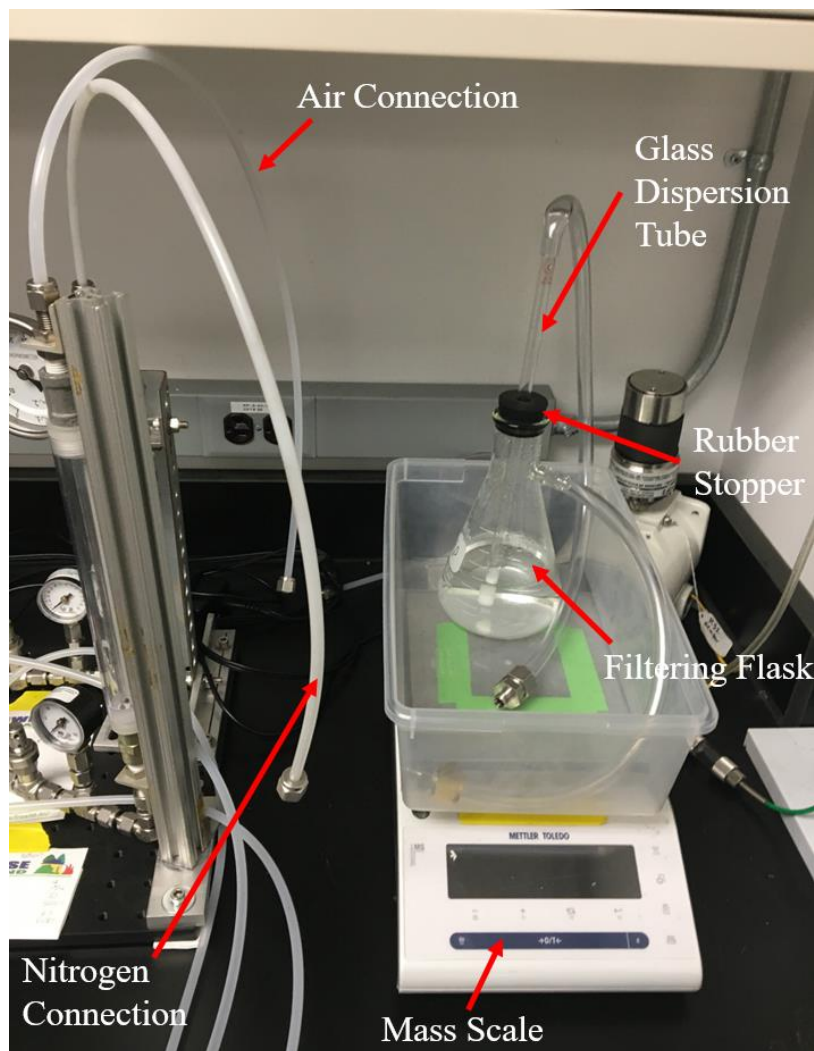


Figure 4.1. Bubbling apparatus.

the thermometer probe to be 22°C. After 60 min, the nitrogen was turned off, the glass dispersion tube was removed, and the filtering flask was weighed again. The weight of the flask after the bubbling is represented by m_2 .

\dot{m}_{exp} was then determined by

$$\dot{m}_{exp} = (m_2 - m_1)/60 \quad (4.7)$$

For a Q_{N_2} of 1 Lpm, \dot{m}_{exp} of water was found to be 0.0143 g/min. Table 4.4 shows the properties of water [21] needed to carry out the calculation to predict \dot{m}_{calc} . The calculated mass loss rate was found to be 0.0199 g/min. Although this value is 39% higher than \dot{m}_{exp} , this is acceptable because the calculation assumes that the incoming nitrogen is perfectly dry, and that the water vapor is perfectly saturated. Because \dot{m}_{exp} is within a reasonable range of \dot{m}_{calc} , this is sufficient proof that experimental mass loss rate values obtained from the mass scale can be used to calculate the necessary contaminant and air flowrates, as opposed to the calculated mass loss rate. \dot{m}_{exp} is preferred because the process of calculating \dot{m}_{calc} assumes perfect theory that is not representative of the actual test process and environment.

Table 4.4. Properties of water.

	$MW_i,$ g/mol	$P_{vap,init},$ bar	$\Delta H_{vap},$ kJ/mol
Water	18.01	0.0233	44.1

For each contaminant, m_{exp} can be determined using the same process that was outlined for water, and equation (4.3) can then be used to determine $Q_{vap,exp}$. The amount of makeup air that is needed to meet X_{test} can be determined from

$$X_{test} = Q_{vap,exp} / (Q_{N_2} + Q_{vap,exp} + Q_{air}) \quad (4.8)$$

Table 4.5 shows the selected properties of each contaminant needed to obtain m_{calc} [21]. Table 4.6 summarizes the mass loss rates and flowrates necessary to reach the desired concentration for each contaminant. The calculated mass loss rates are also included to compare to experimental values. The Q_{N_2} values had to be lowered in order to obtain reasonable Q_{air} values that could be used with the available rotameters. Q_{N_2} values differentiate between the contaminants because different Q_{air} values were needed. Because the flowrates from the contaminants account for less than 0.001% of the total flowrate, Q_{tot} values are nearly identical to those of Q_{air} .

Table 4.5. Properties of contaminants.

	MW_i , g/mol	$P_{vap,init}$, bar	ΔH_{vap} , kJ/mol
<i>n</i> -Heptane	100.2	0.048	36.6
Ethyl acetate	88.11	0.103	35.6
Isopropyl alcohol	60.10	0.044	45.6
Ethanol	46.07	0.079	43.0
Toluene	92.14	0.029	38.0
Trichloroethane	133.4	0.025	32.9
Acetone	58.08	0.247	32.1
Decamethylcyclopentasiloxane	370.8	1.60E-4	49.0
Octamethylcyclotetrasiloxane	296.6	1.30E-3	48.5

Table 4.6. Mass loss rates and flowrates for liquid contaminants.

	Q_{N_2} , Lpm	\dot{m}_{calc} , g/min	\dot{m}_{exp} , g/min	$Q_{vap,exp}$, Lpm	Q_{air} , Lpm
<i>n</i> -Heptane	0.01	2.29E-3	2.20E-3	5.32E-4	1.10
Ethyl acetate	0.003	1.38E-3	1.90E-3	5.22E-4	2.60
Isopropyl alcohol	0.01	1.29E-3	1.20E-3	4.84E-4	2.40
Ethanol	0.005	9.15E-4	6.60E-4	3.47E-4	1.70
Toluene	0.01	1.25E-3	1.60E-3	4.21E-4	2.10
Trichloroethane	0.035	5.36E-3	1.20E-3	2.18E-4	1.10
Acetone	0.003	2.61E-3	5.40E-4	2.25E-4	1.10
Decamethylcyclo- pentasiloxane	0.5	1.39E-3	2.83E-3	1.85E-4	1.40
Octamethylcyclo- tetrasiloxane	0.1	1.80E-3	2.40E-3	1.96E-4	1.90

The contaminants requiring the lowest flowrate of nitrogen were ethyl acetate and acetone, primarily because they have the highest vapor pressures. Liquids with a higher vapor pressure evaporate more easily, so much less nitrogen flow is needed to get the necessary $Q_{vap,calc}$. The silicones have much lower vapor pressures, and therefore require a higher Q_{N_2} to obtain vapor. The calculated flowrates match up very well with the experimental values for some of the contaminants, such as *n*-heptane and isopropyl alcohol. For contaminants such as acetone, the values differ significantly. However, $Q_{vap,calc}$ and Q_{air} are based off the experimental mass loss rate as opposed to the calculated value, so the test concentration is still accurately met.

4.5 Results

Figures 4.2-4.14 summarize the results of the contaminant tests, displayed in the order that the contaminants were tested. Because the sensor's response to both the 10% and 25% LFL of the refrigerant was discussed in Chapter 3, both steady-state voltages are

indicated in the graphs. R-32 was the refrigerant used to monitor the state of health of the sensor following the contaminant test.

n-Butane

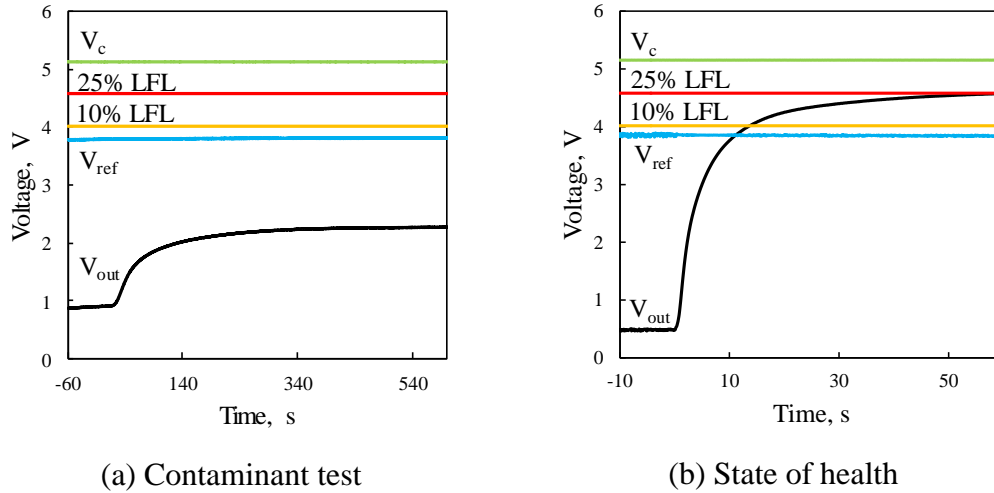


Figure 4.2. Results of the contaminant and state of health test.

Figure 4.2 shows the sensor's response to *n*-butane and the following state of health test. In the contaminant test, V_{out} increased to about 2.3 V before plateauing around 300 s. Although the sensor demonstrated a response to the *n*-butane, it did not surpass the 10% or 25% LFL of R-32, so it would not return a false alarm. In the state of health test, V_{out} reached the 10% LFL in 13.6 s and 25% LFL in 63.2 s. These values show a much slower response time than previously observed, indicating the sensor was poisoned. Although the sensor's health was affected, it was not replaced with a new sensor.

Isopropyl Alcohol

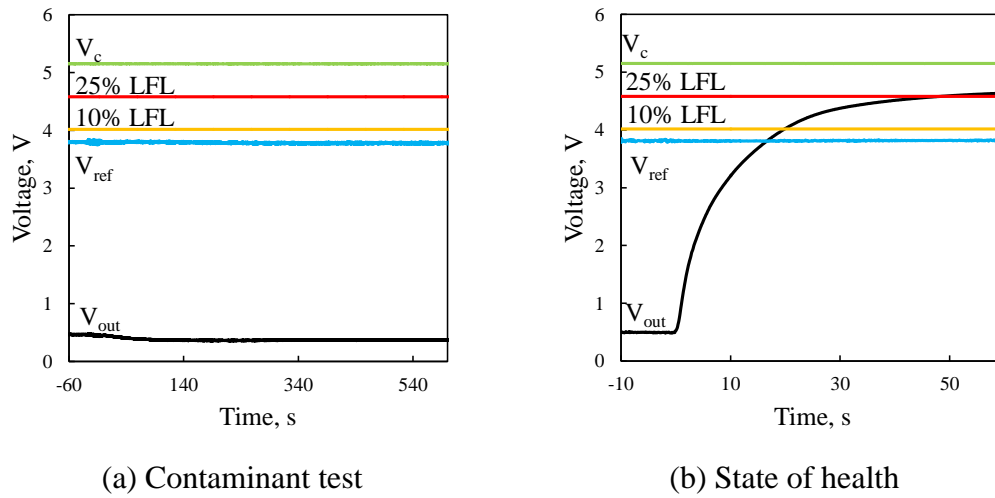


Figure 4.3. Results of the contaminant and state of health test.

Figure 4.3 shows the sensor's response to isopropyl alcohol and the following state of health test. V_{out} decreased slightly by about 0.2 V in 4.3(a). In 4.3(b), V_{out} reached the 10% LFL in 19.9 s and 25% LFL in 48.5 s, indicating the sensor was poisoned.

Ethanol

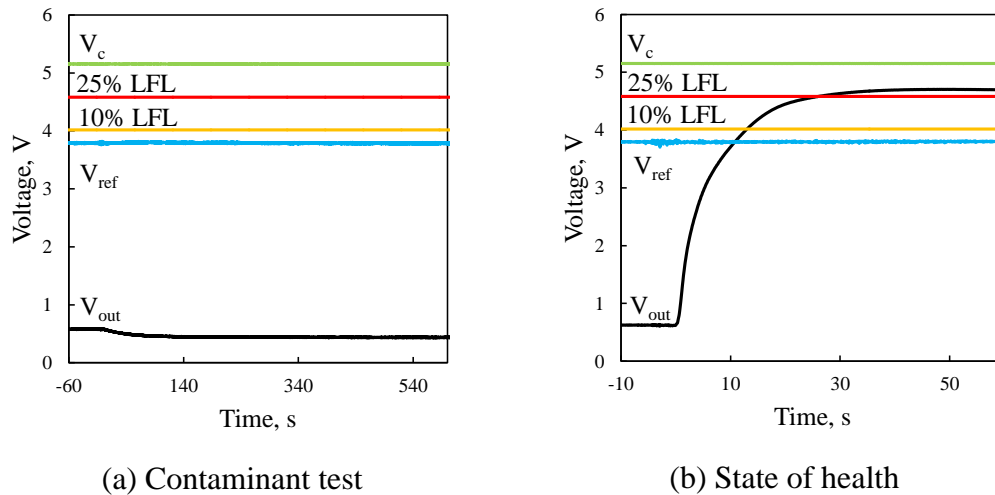


Figure 4.4. Results of the contaminant and state of health test.

Figure 4.4 shows the sensor's response to ethanol and the following state of health test. Similar to the isopropyl alcohol poisoning, V_{out} slightly decreased when exposed to ethanol. However, in the state of health test, V_{out} reached the 10% LFL in 13 s and 25% LFL in 26 s, which is much closer to the response time of a healthy sensor.

Ethyl Acetate

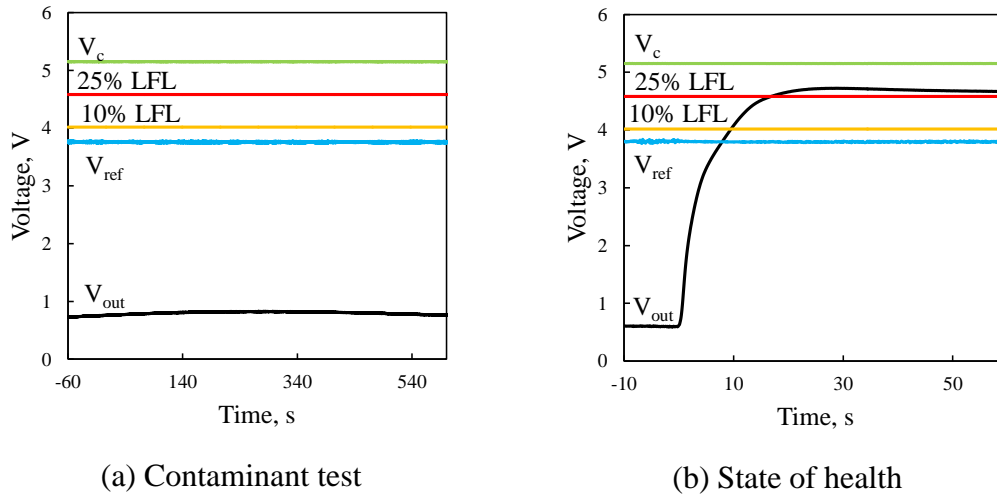


Figure 4.5. Results of the contaminant and state of health test.

Figure 4.5 shows the sensor's response to ethyl acetate and the following state of health test. For ethyl acetate, V_{out} slightly increased about 0.2 V, then interestingly decreased back to the initial voltage. In the state of health test, V_{out} reached the 10% LFL in 9.6 s and 25% LFL in 16.9 s. These values represent the typical response of a healthy sensor. Additionally, this is the first state of health test where there is a slight difference in the shape of the V_{out} curve. After the first 3 s, there is a slight bend in the curve, as opposed to the normal smooth logarithmic curve that is seen in the previous state of health tests.

n-Heptane

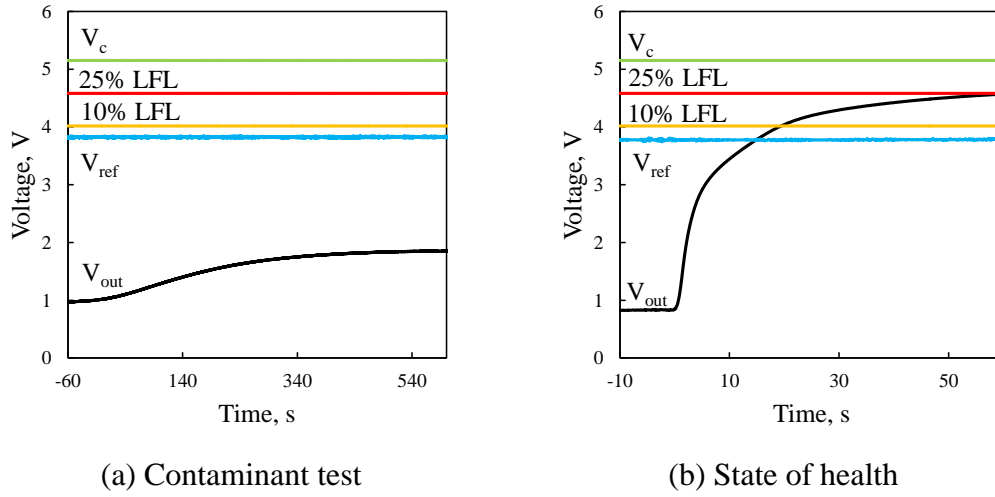


Figure 4.6. Results of the contaminant and state of health test.

Figure 4.6 shows the sensor's response to *n*-heptane and the following state of health test. In 4.6(a), V_{out} plateaued at 1.8 V after about 500 s. 4.6(b) indicates the sensor was poisoned because it took 19.5 s to reach the 10% LFL and 62.8 s to reach the 25% LFL.

Toluene

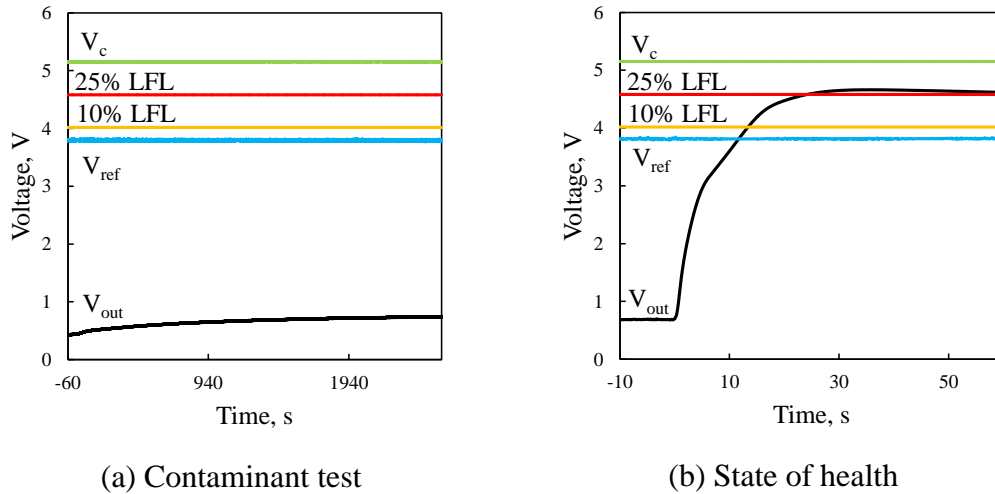


Figure 4.7. Results of the contaminant and state of health test.

Figure 4.7 shows the sensor's response to toluene and the following state of health test. In response to toluene, the sensor voltage continued to rise slightly until about 0.75 V, at which point it stabilized. V_{out} took about 35 min to stabilize, which is over three times longer than the previous tests. In the state of health test, V_{out} reached the 10% LFL in 13.4 s and 25% LFL in 24.3 s, which are fairly close to typical response times. The slight bend in the output voltage curve in the state of health test after an initial few seconds of exposure is much more noticeable. It appears the sensor's ability to respond to the 100% LFL refrigerant concentration is becoming impacted by the contaminant tests, which shows poisoning.

Acetone

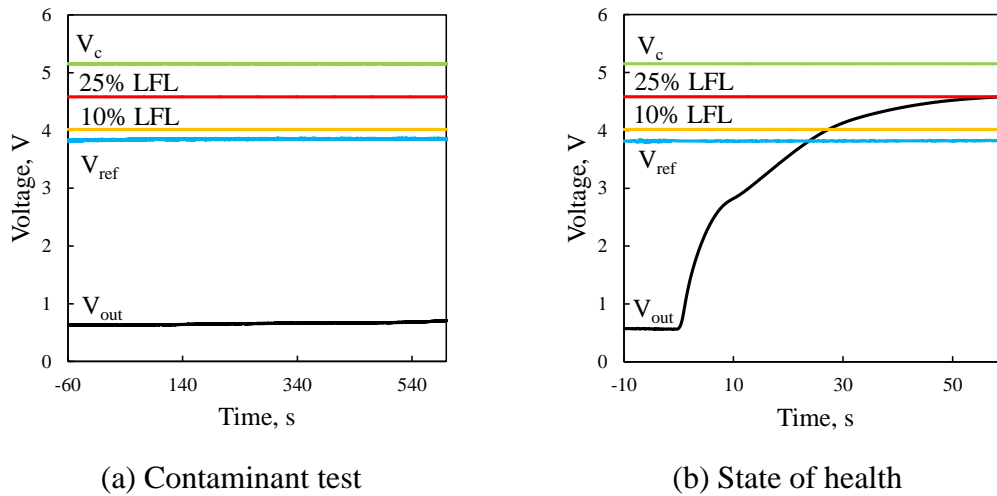
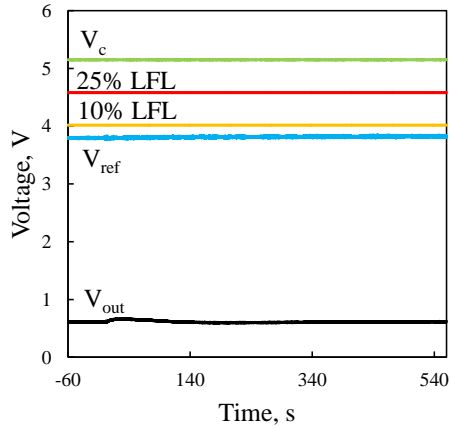


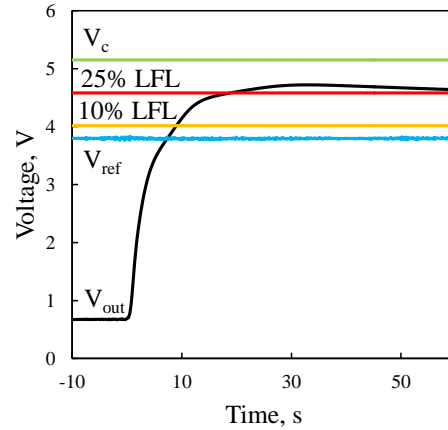
Figure 4.8. Results of the contaminant and state of health test.

Figure 4.8 shows the sensor's response to acetone and the following state of health test. The sensor appeared to have no response to acetone contamination. However, the state of health test shows that the acetone still had an effect on the sensor's response. V_{out} reached the 10% LFL in 27.4 s and 25% LFL in 59.2 s, showing there was poisoning.

Octamethylcyclotetrasiloxane



(a) Contaminant test

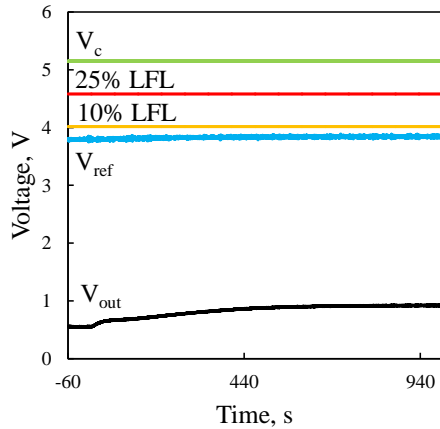


(b) State of health

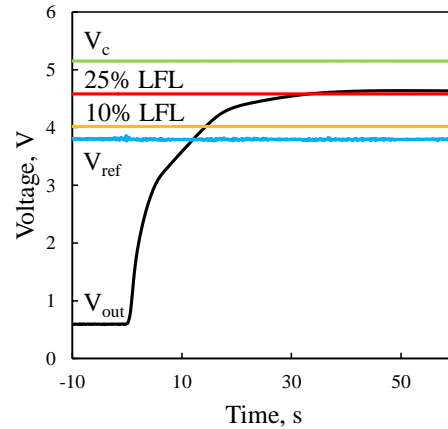
Figure 4.9. Results of the contaminant and state of health test.

Figure 4.9 shows the sensor's response to octamethylcyclotetrasiloxane and the state of health test. There was no response to the silicone. 4.9(b) shows a quick response to the refrigerant, where V_{out} reached the 10% LFL in 9.1 s and 25% LFL in 18.9 s.

Decamethylcyclopentasiloxane



(a) Contaminant test



(b) State of health

Figure 4.10. Results of the contaminant and state of health test.

Figure 4.10 shows the sensor's response to decamethylcyclopentasiloxane and the state of health test. In response to the second of the two silicones, V_{out} rose to 0.9 V and stabilized after about 800 s when contaminated with decamethylcyclopentasiloxane. The response times in the following state of health test were slightly delayed, indicating that poisoning had occurred; V_{out} reached the 10% LFL in 14.4 s and 25% LFL in 33.6 s.

Ammonia

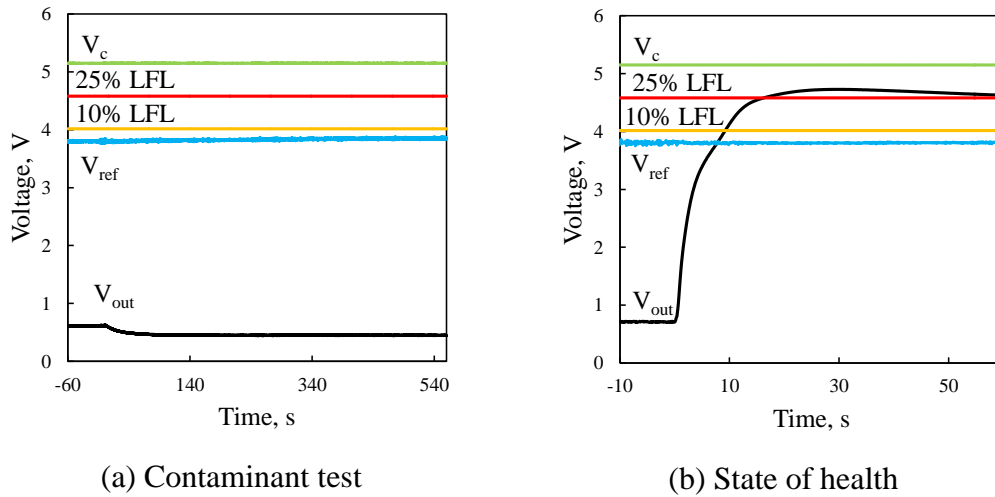


Figure 4.11. Results of the contaminant and state of health test.

Figure 4.11 shows the sensor's response to ammonia and the state of health test. V_{out} decreased by about 0.2 V when it was contaminated with ammonia. The state of health test showed a healthy response, with V_{out} reaching the 10% LFL in 9.3 s and 25% LFL in 16.4 s.

Trichloroethane

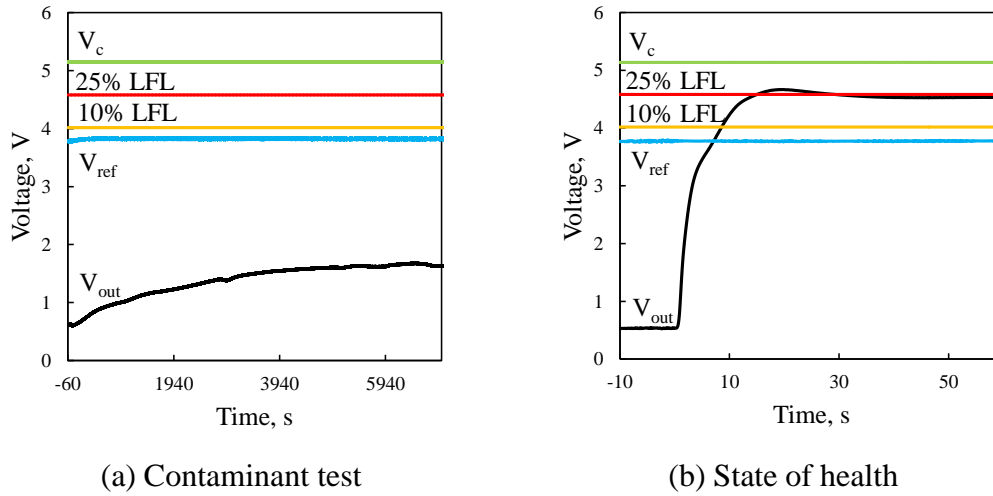


Figure 4.12. Results of the contaminant and state of health test.

Figure 4.12 shows the sensor's response to trichloroethane and the state of health test.

In 4.12(a), V_{out} reached a stable value of about 1.6 V after 100 min of testing. 4.12(b) shows V_{out} reaching the 10% LFL in 8.6 s and 25% LFL in 15 s.

Carbon Dioxide

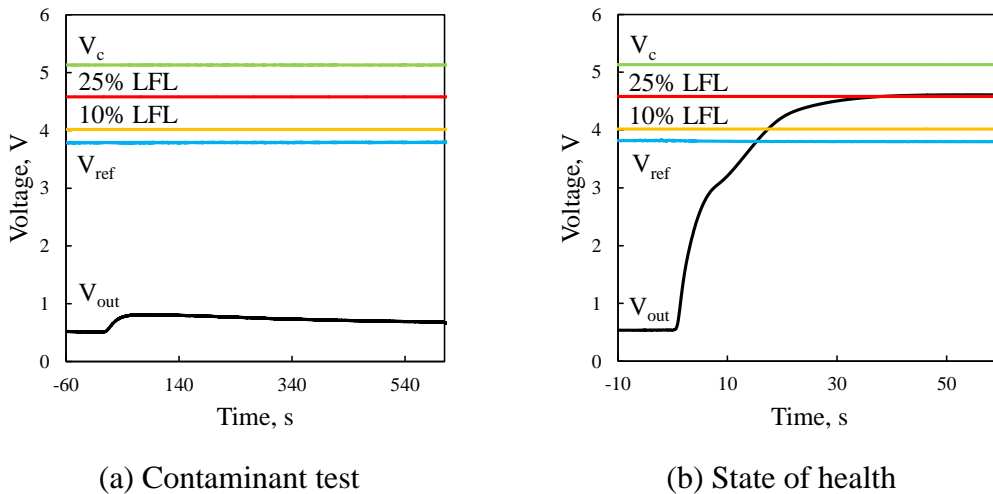


Figure 4.13. Results of the contaminant and state of health test.

Figure 4.13 shows the sensor's response to carbon dioxide and the state of health test. The sensor output voltage for carbon dioxide first increased about 0.3 V, then slowly decreased as the test continued. The state of health test showed the sensor was affected by the carbon dioxide as V_{out} reached the 10% LFL in 17.4 s and 25% LFL in 38.4 s

Methane

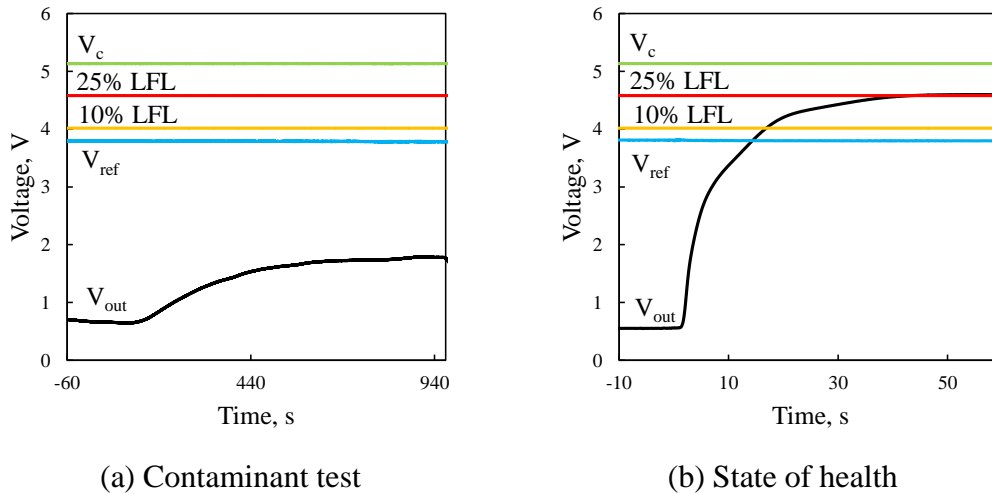


Figure 4.14. Results of the contaminant and state of health test.

Figure 4.14 shows the sensor's response to methane and the state of health test. Methane yielded a stronger response from the sensor with V_{out} rising to about 1.8 V after about 850 s. The delayed response times in the state of health test indicate the sensor was poisoned from the methane; V_{out} reached the 10% LFL in 16.9 s and 25% LFL in 43.7 s

4.6 Discussion of Results

Figure 4.15 summarizes the results of the tests, and is in chronological order of the contaminants tested. According to the output voltage, the sensor was observed to have the strongest response to *n*-butane, followed by *n*-heptane, methane, and trichloroethane. Although the output voltage increased, it did not rise past the 10 or 25% LFL points, so it can be concluded that none of these contaminants will cause a false alarm per UL 60335-2-40 Annex LL. It appears that there is no strong correlation between V_{out} and the response time in the state of health test. V_{out} was very high for trichloroethane, yet the quick response times show no poisoning to the sensor. For acetone, V_{out} was relatively low, yet the response times were fairly slow. There is also no clear correlation between the order in which the contaminants were tested and the

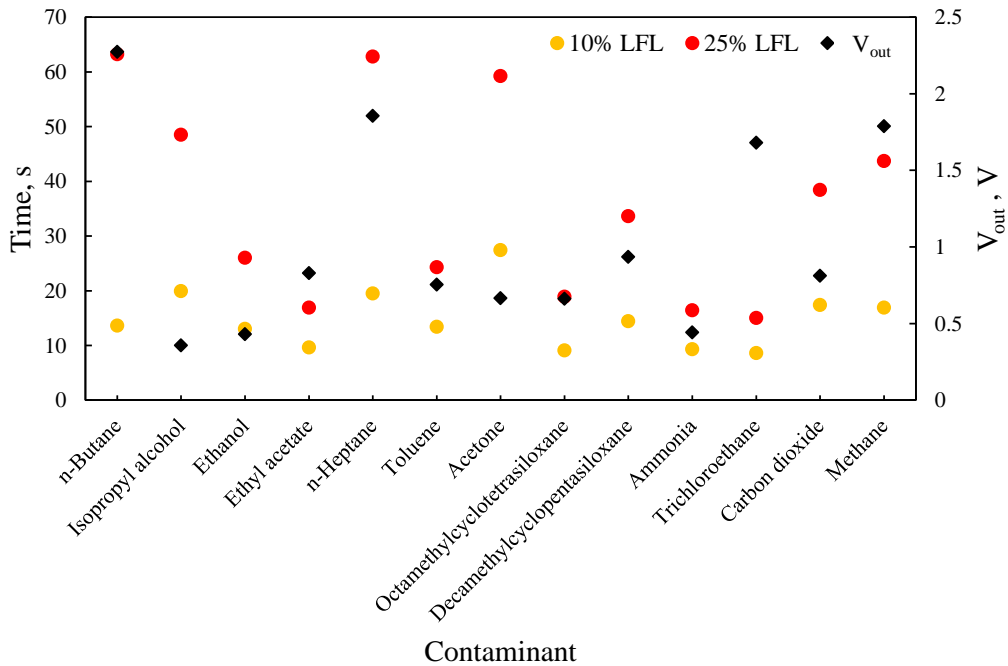


Figure 4.15. Chronological summary of contamination and state of health test results.

response time of the sensor in the following state of health test. In the very first test, the sensor output voltage took over a minute to reach the 25% LFL after being exposed to butane, which is nearly four times as long as the response time of a healthy sensor. However, in the third to last test, the sensor exhibited a healthy response after being exposed to 10 different contaminants. This also shows that the sensor recovered from the poisoning within 24 hours. The sensor exhibited a healthy response in the state of health test following trichloroethane contamination 24 hours after being poisoned by decamethylcyclpentasiloxane. Another possible explanation is that contaminant exposure in between a state of health test with slow response times and a state of health test exhibiting fast response times may have contributed to reducing poisoning in the sensor.

It is certain the sensor was clearly poisoned by a number of the contaminants. Figure 4.16 summarizes only the state of health tests in order of fastest response time to the 10% LFL to slowest. The sensor's response time to both the 10% and 25% LFL equivalent voltage before contaminant testing are indicated for reference. The contaminants can be grouped into three different levels of poisoning effect on the sensor. The first four contaminants all yield a healthy sensor response by showing a response to the 10% LFL within 10 s and to the 25% LFL in under 20 s. The next two contaminants, ethanol and toluene, show mild poisoning. The responses to the 10% LFL are a little higher than 10, and the response to the 25% LFL are below 30 s. The remaining seven contaminants show definite signs of poisoning. While the response times to the 10% LFL slowly increase, the response times to the 25% LFL are all above 30 s.

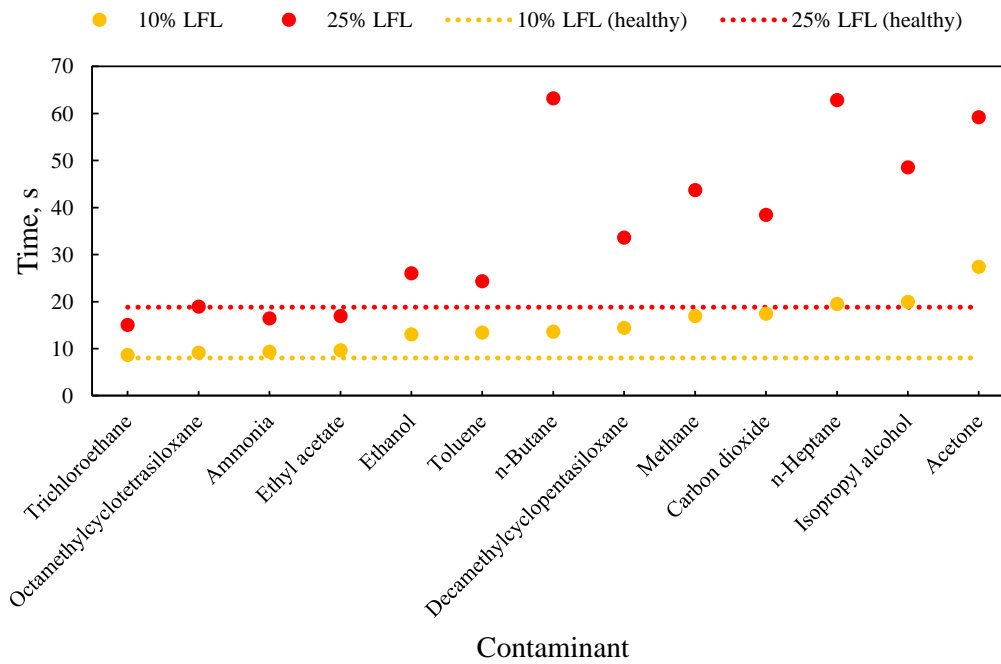


Figure 4.16. Summary of response times from fastest to slowest.

Figure 4.17 shows the response time of the sensor 24 hours following the end of contaminant testing. The response times to the 10% and 25% equivalent voltages

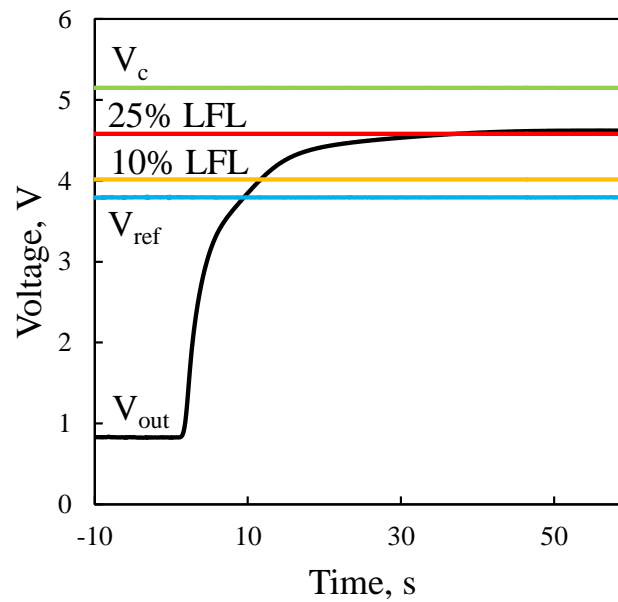


Figure 4.17. Response time following contaminant testing.

were 11.7 and 37.2 s. The response time to the 10% LFL is only slightly slower than that of a healthy sensor, but the response time to the 25% LFL is much slower. This supports the conclusion that the sensor indeed experienced poisoning effects from the contaminants.

Table 4.7 summarizes the effect each contaminant had on the sensor. While none of the contaminants caused the sensor to return a false alarm, all but four of the contaminants caused the sensor's health to deteriorate. Although ethanol and toluene only showed mild poisoning, the slightly slowed response time is still enough to confirm the sensor was affected by these two contaminants.

Table 4.7. Summary of the contaminant's effect on the sensor.

	False Alarm (Y/N)	Deteriorated Health (Y/N)
Trichloroethane	N	N
Octamethylcyclotetrasiloxane	N	N
Ammonia	N	N
Ethyl acetate	N	N
Ethanol	N	Y
Toluene	N	Y
<i>n</i> -Butane	N	Y
Decamethylcyclopentasiloxane	N	Y
Methane	N	Y
Carbon dioxide	N	Y
<i>n</i> -Heptane	N	Y
Isopropyl alcohol	N	Y
Acetone	N	Y

Chapter 5: Conclusions and Future Work

MOS sensors from Figaro were tested to characterize their response time to concentrations of R-32 and R-454B. UL 60335-2-40 Annex LL requires the response time to be under 10 s when exposed to a concentration of 100% of the refrigerant's LFL [5]. It was desired for the alarm set-point to be at the 25% LFL, but unfortunately the sensors could not satisfy the 10 s requirement at this equivalent voltage. When plunged into the refrigerant at a 100% LFL concentration, the average time it took for the sensor voltage to reach what it would output at the 25% LFL was about 17 s. However, the sensor voltage took about 9 s to reach the 10% LFL equivalent voltage, which does satisfy the UL 60335-2-40 Annex LL requirement. It is therefore recommended that the alarm set-point for these sensors be set to the 10% LFL of refrigerant. Although an alarm set-point at 25% of the LFL is more ideal because it would trigger fewer alarms while still providing a comfortable safety factor, the response time is not quick enough for this to be an option.

The time constant, τ , can be determined from the R-32 response time test by

$$e^{(-t/\tau)} = (V_{out} - V_{\infty}) / (V_0 - V_{\infty}), \quad (5.1)$$

where V_{∞} is the steady-state voltage of the sensor and V_0 is the initial voltage of the sensor in ambient air. Figure 5.1 shows the natural log of this relationship fit with a straight line. From the slope of this line, τ can be determined, and is found to be 4.59 s. This value indicates how rapidly the exponential function decays if it had continued to decay at the initial rate. Although τ will vary for different concentrations, it is still well below 10 s.

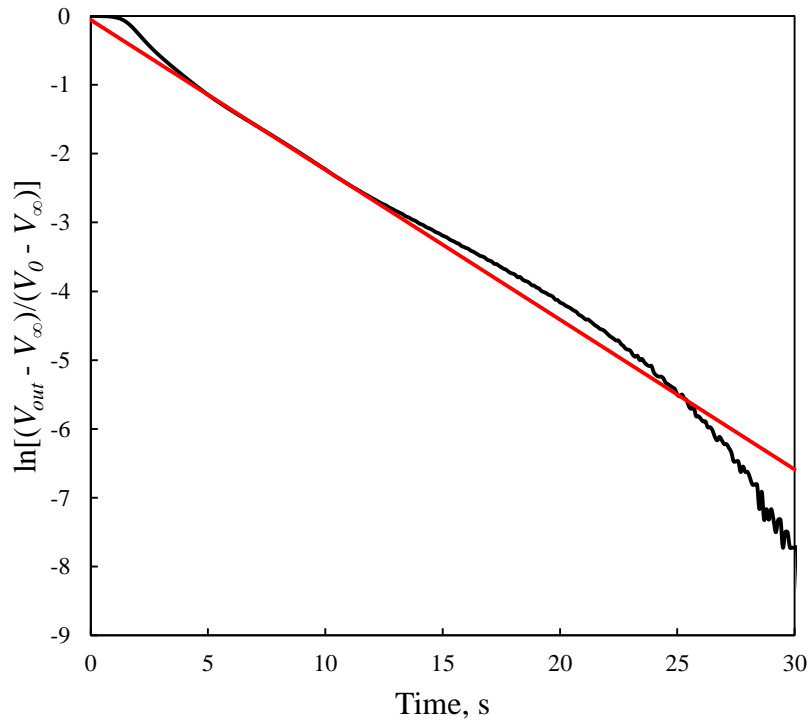


Figure 5.1. Time constant from the R-32 response time test.

The sensors were also tested for their response to a prescribed list of contaminants that are commonly found in commercial/industrial and residential applications. Although some of the contaminants yielded a fluctuation in voltage from the sensor, the change was never enough to return a false alarm. However, the sensor did show signs of poisoning in many cases. While the sensor generally recovered within 24 hours, the sensor failed to produce a healthy response to the refrigerant 1 hour following exposure to the contaminant for 9 of the 13 contaminant tests. Based on these results and concerns about poisoning, Figaro MOS sensors are not recommended for area monitoring detection. However, further studies are needed to better assess MOS sensor suitability for the area monitoring of refrigerant leaks with varying levels of contaminants. These tests need to be repeated according to Annex LL, Section 5 of the

UL standard with 16 hour venting and successive contaminant exposure before final assessment of poisoning.

Future work could focus on continuing testing with the Figaro MOS sensor to corroborate these findings with more data. Testing with all the contaminants as pre-diluted gases, like the ammonia, would likely yield more accurate results than the bubbling method used, but can be quite expensive. The velocity of refrigerant in the test vessel could also be varied. If the gas were to diffuse past the mesh filter, the response time slows considerably because refrigerant molecules adsorb onto the MOS. This could be a motivation to add an additional alarm state based on the rate of rise. Multiple sensors could be used for running the contaminant tests per full Section 5 of Annex LL. Multiple new sensors could also be used for each contaminant to pinpoint qualitatively what the poisoning effect of each is. However, these options would involve a lot more sensors which requires much more time and money. Finally, future testing could include modest concentrations of refrigerant with modest concentrations of contaminant. It is unlikely that the sensor would only be exposed to one or the other during its actual course of operation. Being exposed to small concentrations of both at the same time is much more representative of what would be expected in the environment.

It is likely that other sensing technologies will need to be explored. IR was the other technology that was determined to have good potential. Because of how the technology works, they would not have the poisoning issue that the MOS sensors have. Also, the prices will drop as more units are produced, so IR sensors will likely be the dominant technology in the near future for A2L refrigerant detection.

Bibliography

- [1] FETA. An Introduction to A2L Refrigerants and Their Use in Refrigeration, Air Conditioning and Heat Pump applications. Technical report, Federation of Environmental Trade Associations, 2017.
- [2] M. Wagner and R. Ferenchiak. Leak Detection of A2L Refrigerants in HVACR Equipment. Technical report, Air-Conditioning, Heating and Refrigeration Technology Institute, 2017.
- [3] Danfoss. *Application Guide for Gas Detection in Refrigeration Systems*, 2007.
- [4] *Pre-Calibrated Module for Refrigerant Gas r-32*. FCM2630-C00. Figaro Engineering Inc. Apr 2019.
- [5] UL. Standard 60335-2-40. Household And Similar Electrical Appliances – Safety – Part 2-40: Particular Requirements for Electrical Heat Pumps, Air-Conditioners and Dehumidifiers. Technical report, Underwriters Laboratory, 2019.
- [6] G. Fine, L. Cavanagh, A. Afonja, and R. Binions. Metal Oxide Semi-Conductor Gas Sensors in Environmental Monitoring. *Sensors*, 10:5469-5502, 2010.
- [7] C. Wang, L. Yin, L. Zhang, D. Xiang, and R. Gao. Metal Oxide Gas Sensors: Sensitivity and Influencing Factors. *Sensors*, 10:2088-2106, 2010.
- [8] *Air Quality Click*. MIKROE-1630. Ver. 1.00. MIKROE.
- [9] Adafruit. Adafruit MiCS5524 CO, Alcohol and VOC Gas Sensor. <https://www.adafruit.com/product/3199#technical-details>. Accessed: 2020-03-28.
- [10] Honeywell. Honeywell Manning VL. <https://www.honeywellanalytics.com/en/products/Manning-VL>. Accessed: 2020-03-28.
- [11] IPCC. Changes in Atmospheric Constituents and in Radiative Forcing. *Climate Change 2007: The Physical Science Basis*, 212, 2007.
- [12] ASHRAE. Standard 34-2013, Designation and Safety Classification of Refrigerants. Technical report, American Society of Heating, Refrigerating and Airconditioning Engineers, Atlanta, 2013.
- [13] H. Pham and R. Rajendran. R32 And HFOs As Low-GWP Refrigerants For Air Conditioning. *International Refrigeration and Air Conditioning Conference*, Paper 1235, 2012.
- [14] M. Smith. California Refrigerant Regulations Overview. Technical report, North American Sustainable Refrigeration Council, 2019.
- [15] D. McClure and T. Anderson. A Comparison of Refrigerant Constant Monitoring Leak Detectors. *International Refrigeration and Air Conditioning Conference*, Paper 115, 1990.

- [16] R. Tapscott and C. Sohn. Halocarbon Refrigerant Detection Methods. Technical report, US Army Construction Engineering Research Laboratories, Champaign, Illinois, 1996.
- [17] G. Korotcenkov. Metal oxides for solid-state gas sensors: What determines our choice? *Materials Science and Engineering B*, 139:1-23, 2007.
- [18] X. Liu, S. Cheng, H. Liu, S. Hu, D. Zhang, and H. Ning. A Survey on Gas Sensing Technology. *Sensors*, 12:9635-9665, 2012.
- [19] *Difluoromethane*; SDS No.: 000010021734 [Online]; Linde Gas GmbH: Carl-von-Linde-Platz 1, Austria, Nov 26, 2018.
- [20] *R-454B*; SDS No.: 1354822-00035 [Online]; Chemours: Baanhoekweg 22, Netherlands, Dec 1, 2017.
- [21] P.J. Linstrom and W.G. Mallard, Eds., *NIST Chemistry WebBook, NIST Standard Reference Database Number 69*, National Institute of Standards and Technology, Gaithersburg MD, <https://doi.org/10.18434/T4D303>. Accessed: 2020-03-28.